Published in final edited form as:

Cell Rep. 2022 May 03; 39(5): 110765. doi:10.1016/j.celrep.2022.110765.

HIV Tat and cocaine interactively alter genome-wide DNA methylation and gene expression and exacerbate learning and memory impairments

Xiaojie Zhao[1,2,5,6,7], **Fan Zhang**[3,7], **Suresh R. Kandel**[1,2], **Frédéric Brau**[4], **Johnny J. He**[1,2,5,8,*]

[1]Department of Microbiology and Immunology, Chicago Medical School, Rosalind Franklin University, North Chicago, IL 60064, USA

[2]Center for Cancer Cell Biology, Immunology and Infection, Rosalind Franklin University, North Chicago, IL 60064, USA

[3]Department of Family Medicine, University of North Texas Health Science Center, Fort Worth, TX, USA

[4]Université Côte d'Azur, CNRS, IPMC, Sophia-Antipolis 06560, France

[5]School of Graduate and Postdoctoral Studies, Rosalind Franklin University, North Chicago, IL 60064, USA

[6]Present address: Center for Psychiatric Genetics, NorthShore University Health System, Evanston, IL 60201, USA and Department of Psychiatry and Behavioral Neurosciences, University of Chicago, Chicago, IL 60637, USA

[7]These authors contributed equally

[8]Lead contact

SUMMARY

Cocaine use is a major comorbidity of HIV-associated neurocognitive disorder (HAND). In this study, we show that cocaine exposure worsens the learning and memory of doxycycline-inducible and brain-specific HIV Tat transgenic mice (iTat) and results in 14,838 hypermethylated CpG-related differentially methylated regions (DMRs) and 15,800 hypomethylated CpG-related DMRs, which are linked to 52 down- and 127 upregulated genes, respectively, in the hippocampus of iTat mice. These genes are mostly enriched at the neuronal function-, cell morphology-, and synapse formation-related *extracellular matrix (ECM) receptor-ligand interaction* pathway and mostly

*Correspondence: johnny.he@rosalindfranklin.edu.

AUTHOR CONTRIBUTIONS

X.Z., F.Z., and J.J.H. conceived and supervised all studies. X.Z. and J.J.H. designed all animal experiments. X.Z. and S.R.K. preformed all animal experiments. F.Z., X.Z., and J.J.H. designed and performed bioinformatic analysis. X.Z. and F.B. analyzed all staining images. X.Z., F.Z., S.R.K., F.B., and J.J.H. interpreted all results. X.Z., F.Z., and J.J.H. wrote the manuscript with input from all other authors.

SUPPLEMENTAL INFORMATION

Supplemental information can be found online at https://doi.org/10.1016/j.celrep.2022.110765.

DECLARATION OF INTERESTS

The authors declare no competing interests.

impacted in microglia. The accompanying neuropathological changes include swollen dendritic spines, increased synaptophysin expression, and diminished glial activation. We also find that sex (female) and age additively worsen the behavioral and pathological changes. These findings together indicate that chronic cocaine and long-term Tat expression interactively contribute to HAND, likely involving changes of DNA methylation and ECM receptor-ligand interactions.

Graphical abstract

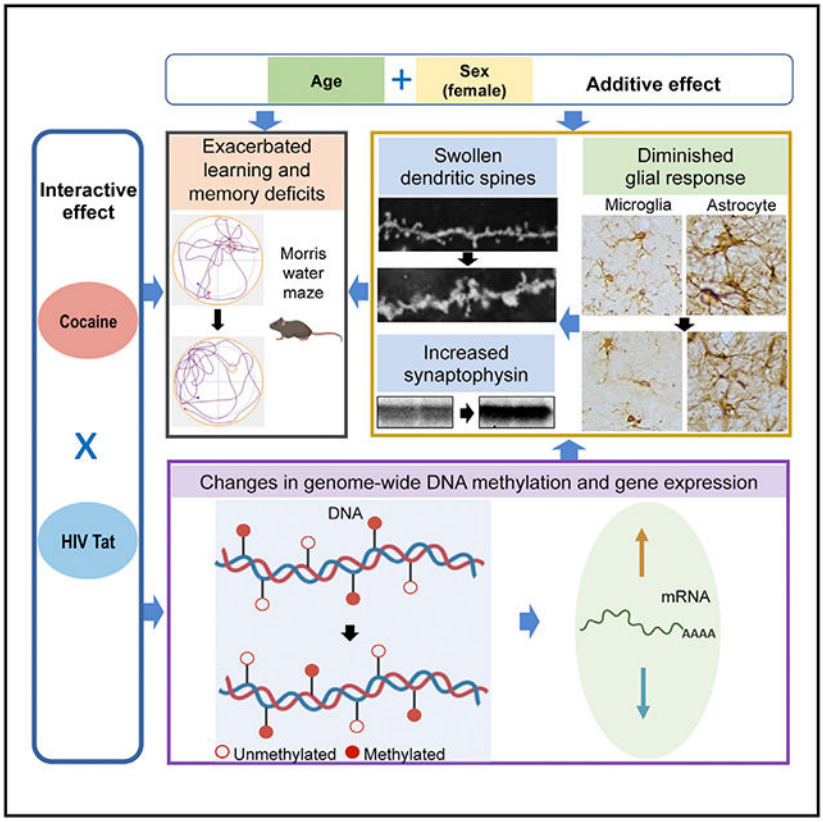

In brief

Zhao et al. investigate combined effects of HIV Tat and cocaine on HIV-associated neurocognitive disorder and the underlying molecular mechanisms, using doxycycline-inducible and brain-specific HIV Tat transgenic mice. They uncover specific changes in behavior, neuropathologies, genome-wide DNA methylation, gene expression, and processes affected by combined cocaine and Tat.

INTRODUCTION

HIV infection of the central nervous system (CNS) occurs in a majority of HIV-infected individuals and causes HIV-associated neurocognitive disorder (HAND) in up to 50% of the infected population (Egger et al., 2002; May et al., 2007; Moreno et al., 2000). One of the major pathogenic factors for HAND is HIV viral protein Tat. Tat is secreted from HIV-infected microglia/microphages and astrocytes (Westendorp et al., 1995; Xiao et al.,

2000) and is detected in the CNS of HIV-infected individuals (Hudson et al., 2000; Wiley et al., 1996). Tat continues to be expressed in HIV-infected individuals whose HIV replication is effectively suppressed by combination antiretroviral therapy (cART) (Henderson et al., 2019; Hudson et al., 2000; Johnson et al., 2013). Recombinant Tat protein, when given *in vivo*, and Tat expression alone in the doxycycline (Dox)-inducible brain-specific HIV Tat transgenic mice (iTat) results in neurological and neuropathological changes reminiscent of those noted in the HIV-infected brain (Jones et al., 1998; Kim et al., 2003; Paris et al., 2014). The controllability of the time and duration of Tat expression in the iTat model offers a great opportunity to investigate long-term effects of Tat in the context of HIV infection treated with cART and comorbidities such as chronic substance use disorders.

Cocaine use is prevalent in the HIV-infected population (Kumar et al., 2015; Meade et al., 2018; Shu et al., 2020). Cocaine impairs the cellular functions and promotes HIV replication (Baldwin et al., 1997; Klein et al., 1993), disrupts the integrity of the blood-brain barrier (Kousik et al., 2012; Sharma et al., 2009; Yao et al., 2011), induces upregulation of pro-inflammatory mediators and neuroinflammation (Clark et al., 2013; Fox et al., 2012), and facilitates the progression of HAND (Litvin et al., 2019; Martin et al., 2018; Meyer et al., 2014). Cocaine also alters histone modifications through HDAC, sirtuin, and G9a, and transcriptional regulation of genes, such as FosB, CDK5, and BNDF, at the chromatin level, which contributes to the development and maintenance of addiction (Nestler, 2014; Renthal and Nestler, 2008; Rogge and Wood, 2013). Furthermore, cocaine upregulates miR-212, leading to an amplification of the stimulatory effects of cocaine on CREB signaling (Jonkman and Kenny, 2013). A number of studies have documented interactive effects between cocaine and Tat. Tat potentiates the psychostimulant effects of cocaine and heightens drug award (Napier et al., 2014; Paris et al., 2014). Tat and cocaine alter metabolism (Cotto et al., 2018b; Mohseni Ahooyi et al., 2018; Sivalingam et al., 2021) and increase the blood-brain barrier permeability (Gandhi et al., 2010; Sun et al., 2016; Yao et al., 2012). However, these studies are performed using recombinant Tat protein *in vitro* or short-term Tat expression *in vivo*, and little is known about whether chronic cocaine use results in epigenetic changes, specifically DNA methylation in the context of long-term Tat expression and whether these changes contribute to HAND neurology and neuropathology.

In the study, we determined the effects of chronic cocaine exposure and long-term Tat expression on neurological, DNA methylation, and neuropathological changes. We fed iTat mice with Dox to induce Tat expression for 5 and 11 months, exposed these mice to cocaine for 2 weeks, kept them drug free for 10 days, and performed behavioral assessments. At the end of behavioral tests, we euthanized the animals and collected brain tissues to isolate genomic DNA for single-base resolution whole-genome bisulfate sequencing, to isolate RNA for RNA sequencing and to perform neuropathology. We then used system biology to characterize the gene expression, and biological pathways and processes altered by cocaine and Tat as well as the relationship among DNA methylation change-associated gene expression, and biological pathways and processes, neurology, and neuropathology.

RESULTS

Cocaine exposure worsened learning and memory impairments by Tat

Following weaning iTat mice were fed with Dox for 5 and 11 months (Figure 1A), injected cocaine (Coc) (30 mg/kg/day) for 14 days (Morrell et al., 2011; Park et al., 2013; Pope et al., 2016), kept drug-free for 10 days, and subjected to a battery of behavioral tests. Wild-type (WT) mice and saline (Sal)-treated mice were included as the controls for iTat mice and Coc, respectively. Behavioral tests were performed in the order of increasing stress level, namely elevated plus maze (EPM) for anxiety, open-field test (OPT) for locomotor activity and anxiety, rotarod test (RT) for balance and coordination, tail suspension test (TST), forced swim test (FST) for depressive status, and Morris water maze (MWM) for learning and memory.

During the 5-day MWM training, iTat mice showed longer escape latency trend than WT mice in the absence of Coc; Coc prolonged escape latency in iTat mice while it only slightly shortened escape latency in WT mice (Figure 1B). Cumulative distance showed the same pattern, but with the more pronounced impact of Tat on 6-month (6m) females (Figure S1A; Table S1); 12m females had less pronounced effects of Tat and Coc than males of 6m and 12m and 6m females. For the first probe test (short-term memory), which was performed 1 day after the last training, iTat 6m males showed shorter time at platform and fewer platform events than WT 6m males, and Coc showed shorter latency to platform in all iTat mice than WT mice, less time at target quadrant in iTat males than WT males of both 6m and 12m groups, and shorter distance to target quadrant in iTat 12m males than WT 12m males (Figure 1C). In addition, Coc showed shorter time at target quadrant and shorter distance to target quadrant than Sal in iTat males. For the second probe test, which was performed 7 days after the first probe test for long-term memory, iTat mice showed shorter time at target quadrant than in WT in 6m females and 12m males, shorter time at platform, fewer platform events, shorter distance to target quadrant, and shorter distance to platform than WT in 12m males when given Coc, and iTat showed longer latency to platform than WT in 12m males, regardless of Coc or Sal treatment (Figure S1B). In addition, Coc showed longer distance to target quadrant than Sal in iTat males.

For EPM, iTat showed more open arm entries than WT in 6m males and 6m females, longer open arm time than WT in 12m males, and longer open arm distance than WT in 12m males (Figure S2A; Table S2). Coc showed more open arm entries and longer open arm distance than Sal in iTat 6m, WT 6m females, and iTat 12m of both males and females. For OPT, measured by total distance and maximum speed for locomotor activity, and central distance and central entries for anxiety, iTat showed shorter total distance than WT in 12m females, lower maximum speed than WT in 6m females and 12m females, longer central distance than WT in 12m males, and more central entries than WT in 12m males (Figure S2B). Coc showed shorter longer total distance than Sal in iTat 6m females, higher maximum speed than WT in iTat 12m females, longer central distance than Sal in iTat 6m females and WT 12m males, and more central entries than Sal in 6m females of both WT and iTat. For RT, measured by latency to fall for balance and coordination ability, iTat showed shorter latency to fall than WT in 6m females at the speed of 30 rpm, Coc showed longer latency to fall

than Sal in 12m females (Figure S2C). For TST and FST, measured by immobile time for depressive status, Coc showed shorter immobile time of TST than Sal in iTat 12m females (Figure S2D) and shorter immobile time of FST than Sal in WT 12m females (Figure S2E). In addition, iTat showed shorter immobile time of FST in 6m males than WT, regardless of Coc or Sal treatment.

Age and sex independently contributed to behavioral abnormalities by Tat and cocaine

Similar patterns of learning and memory and cellular response to Tat and cocaine were noted among all four groups of 2 ages × 2 sexes: 6m males, 6m females, 12m males, and 12m females (Tables S1, S3, and S4). To further ascertain if age and sex had different learning and memory and cellular response to Tat and cocaine, we performed statistical analysis for comparisons among these four groups (Table S5). In learning and memory of MWM, 12m females had longer escape latency and cumulative distance than 6m females, and 12m females showed longer escape latency and cumulative distance than 12m males, suggesting that the learning and memory of females are more vulnerable to aging.

Chronic exposure led to significant changes in genome-wide DNA methylation in the presence of Tat

Next, we performed the whole-genome bisulfate sequencing (WGBS) with single-base resolution and determined the impact of chronic cocaine and long-term Tat on genome-wide DNA methylation, focusing on methylated cytosine adjacent to a guanine (CpG) or another three nucleotides, adenine, thymine, and cytosine (CpH). We chose hippocampus (HIP) hemispheres from the mice of eight 12m groups, selected three samples from each group, and extracted their DNA for 24 WGBS libraries, as HIP and 12m were the brain region and age that were most noted for the changes in learning and memory by cocaine and Tat. Using the threshold of a minimum of six reads per mC site, we identified a total of 39,312,240 CpG and 149,800,650 CpH sites. Initial analysis did not indicate any significant differences in the number and distribution of mC sites between males and females (Y chromosomes were excluded from analysis), which was consistent with our behavioral findings that both males and females showed generally similar trends in their learning and memory response to cocaine and Tat. Therefore, we decided to combine males and females to have four groups and focus on two factors: cocaine and Tat (Figure S3).

We first compared the average methylation level of each CpG site among four groups. Cocaine showed lower mCpG than Sal in WT mice, while iTat showed higher mCpG than WT in Sal. In addition, there was still a significant interaction between Tat and cocaine, despite their trade-off effects (Figure 2A). The mCpG sites showed similar distribution patterns in all 20 chromosomes among these 4 groups (Figure 2B). To further identify differentially methylated regions (DMRs), we framed 6 continuous mC sites as a calculated unit in preset regions and used the linear mixed model to determine the methylation value (M value) in three comparisons, including WT-Sal versus iTat-Sal (Tat factor), WT-Sal versus WT-Coc (Coc factor), and interaction (Tat × Coc factor), which was used to capture unexpected changes in present of both Tat and Coc factors. For mCpG-related DMRs, 18,371 hypermethylated DMRs (Hyper-DMRs) and 20,195 hypomethylated DMRs (Hypo-DMRs) were identified for Tat (left panel, Figure 2C); 22,269 Hyper-DMRs and 34,308

Hypo-DMRs were identified for Coc (left panel, Figure 2D); and 14,838 Hyper-DMRs and 15,800 Hypo-DMRs were identified for Tat × Coc (left panel, Figure 2E). Next, we traced these significant DMRs back to chromosomes and located the four lowest numbers of DMRs at chromosomes 16, 18, 19, and X, and the four highest numbers at chromosomes 2, 5, 7, and 11, across these four groups (right panels, Figures 2C and 2D). These results were consistent with the chromosome distribution of mouse active genes (Cross et al., 1997), indicating that the impact of Tat, Coc, or Tat × Coc on chromosomes is broad and non-selective. Finally, we intersected the significant DMRs of these three comparisons and found that 5,232 DMRs were overlapped in all of them, and 21,292, 36,744, and 11,541 DMRs were unique to Tat, Coc, and Tat × Coc, respectively (Figure 2F).

We also performed analysis of the average methylation level of each CpH site and chromosome distribution and obtained similar findings to CpG (Figures S4A and S4B). We then did the similar CpH-related DMR analysis. The total numbers of CpH-related Hyper-DMRs and Hypo-DMRs were lower than CpG-related Hyper-DMRs and Hypo-DMRs. Totals of 9,234 Hyper-DMRs and 3,055 Hypo-DMRs were identified for Tat (left panel, Figure S4C), 4,427 Hyper-DMRs and 7,714 Hypo-DMRs were identified for Coc (left panel, Figure S4D), and 1,995 Hyper-DMRs and 2,762 Hypo-DMRs were identified for Tat × Coc (left panel, Figure S4E). Chromosomes 16, 18, 19, and X had the lowest CpH-related DMR distribution for all factors, which was similar to CpG-DMRs (right panels, Figures S4C and S4D). However, the four highest CpH-related DMRs for these three factors showed different chromosomes, which were 1, 2, 4, 5, 6, and 7. There were 898 CpH-related DMRs overlapped in all three factors, and 8,813, 8,850, and 1,860 CpH-related DMRs were unique to Tat, Coc, and Tat × Coc, respectively (Figure S4F). We also investigated the distribution of CpG DMRs among promotors, exons, and introns relative to genomic distribution. However, no significant differences were found, even though the intron regions showed higher convergent tendency across three comparisons (upper panels, Figure S5A). Similar findings were noted for CpH-related DMRs for all three factors (lower panels, Figure S5A).

Alterations of genome-wide gene expression by Tat and cocaine

To determine changes of gene expression resulting from the changes of DNA methylation by cocaine and Tat and their relationship with the behavioral and cellular response to Tat and cocaine, we isolated RNA from the other corresponding HIP hemispheres of the same mice and performed bulky RNA sequencing (RNA-seq). We used the same linear mixed model and identified differentially expressed genes (DEGs) among these four groups and linked them with DMRs (Figure S3). In CpG-related DMRs, Tat altered 20,437 genes containing or proximal to Hyper-DMRs and 22,583 for Hypo-DMRs, of which 5,184 genes were overlapped; for Coc, 24,796 genes were containing or proximal to Hyper-DMRs, 32,759 genes for Hypo-DMRs, and 8,701 genes for both; for Tat × Coc, 17,950 genes were containing or proximal to Hyper-DMRs, 18,518 genes for Hypo-DMRs, and 3,959 genes for both (Figure 3A; Table S6). In addition, 513, 242, and 432 upregulated DEGs (Up-DEGs) and 506, 479, and 186 downregulated DEGs (Down-DEGs) were identified by Tat, Coc, and Tat × Coc, and 140, 79, and 127 Up-DEGs were linked to CpG-related Hypo-DMRs and 143, 143, and 52 Down-DEGs were linked to CpG-related Hyper-DMRs under Tat, Coc, and

Tat × Coc factor, respectively. The differences among all four overlaps, Hyper-DMRs and Up-DEGs, Hyper-DMRs and Down-DEGs, Hypo-DMRs and Up-DEGs, and Hypo-DMRs and Down-DEGs under Tat, Coc, and Tat × Coc factors reached statistical significance by using Fisher's exact test.

Next, we performed GO and KEGG enrichment analysis on these overlapped genes to determine whether there were any specific functions or pathways involved. Tat, Coc, and Tat × Coc had different top 10 functional clusters ($p < 0.05$) from GO functional analysis (Figure 3B; Table S7). The cluster with the largest gene ratio and gene counts for Tat was *Carbohydrate derivative binding*, for Coc it was *cell surface receptor signaling pathway*, and for Tat × Coc it was *nervous system development*. Several morphology-related clusters were overlapped between Coc and Tat × Coc, such as *cell projection morphogenesis*, *cell part morphogenesis*, and *cell projection organization*, suggesting that cocaine plays a pivotal role in inducing pathological changes (middle and right panels, Figure 3B). More neuron functional clusters occurred in Tat × Coc, including *neuron projection development*, *neuron development*, *neurogenesis*, and *dendrite development* (right panel, Figure 3B), which provides molecular evidence to support our behavioral findings that chronic cocaine use led to more severe cognition decline in iTat mice. Different to GO functional clusters, KEGG pathway analysis revealed more convergent effects among these three factors, as the *extracellular matrix (ECM) receptor-ligand interaction* pathway was found in all of them (Figures 3C and S5D). ECM is deeply involved in synapse formation and plasticity (Ferrer-Ferrer and Dityatev, 2018). These findings suggest that Tat, Coc, and Tat × Coc affect neuronal function commonly through the *ECM receptor interaction* pathway.

To determine the roles of different cell types in response to Tat and cocaine, we employed machine learning to build up the database of different brain cell types and then used this database to tag the above overlapped genes into neuron, microglia, astrocyte, oligodendrocyte, oligodendrocyte progenitor cell (OPC), and endothelial cell. Specifically, we took the top 6,000 ranked cell-type-enriched mouse genes (McKenzie et al., 2018), mapped them with the RNA-seq transcriptome database from purified brain cells (Zhang et al., 2014), employed a support vector machine (Zhang et al., 2021) to build a learning model with these mapped genes, and applied the trained model to predict the cell type for the unmapped genes. The largest numbers of genes were in microglia for all three factors (Figure 3D), suggesting that microglia was the most affected cell type by Tat, Coc, and Tat × Coc. All the other five cell types appeared to be somewhat equally affected among these three factors.

To identify the most promising gene targets for the morphological changes of microglia, astrocyte, and neuron and mouse behavior, we used a volcano map to sort out genes with $q < 1e\text{-}5$ DMRs and $q < 0.01$ DEGs (marked in red in Figure 3E) and heatmap to document these 20 top-ranked genes in microglia and the 10 top-ranked genes, if there were any, in astrocytes and neurons with $q < 0.05$ DEGs (Figure 3F). The genes marked in red in the volcano map were highlighted with the same color in the heatmap, and these genes had the highest significance in both DNA methylation and gene expression by Tat, Coc, and Tat × Coc. Downregulation of *Ranbp17* and *Vars2* and upregulation of *Abca8b, Olfr558, Asap2*, and *Acaa1b* in microglia, and *Sec61a2f* in neurons, were highly involved in Tat-induced

behavioral and pathological changes; for Coc, downregulation of *Col6a1, Slco4c1, Vwa5b1, Asap2, Smc2, Gpr157, Map3k13*, and *9330182L06Rik* in microglia, *Ptpn9* in astrocytes, and *Yeats4* in neurons, and upregulation of *Atp8a2* and *Rcc1* in microglia; and for Tat × Coc, downregulation of gene *Ift172, Eif2ak4, Pik3c2a*, and *Phf8* in microglia, *Garem1* and *Adgrb3* in astrocytes, and *Dcun1d4* and *Adgrb3* in neurons.

Other genes that were not highlighted in heatmap could also play an important role in behavioral and cellular changes by these three factors, as they all reached significant standards of DMRs ($q < 0.05$) (Figure 3F). Of particular note was that several genes were present in at least two of these three factors: Tat, Coc and Tat × Coc. In microglia, *Ift172* and *Eif2ak4* were downregulated in Tat × Coc, but shown to be upregulated in Coc. *Slco4c1* was shown to be upregulated in Tat × Coc, but downregulated in Coc; and *Asap2* was shown to be upregulated in Tat and Tat × Coc but downregulated in Coc. In astrocytes, *Garem1* was downregulated in Tat × Coc, but upregulated in Coc. In neurons, *Dcun1d4* and *Prune2* were up- and downregulated, respectively, in both Tat × Coc and Tat, but to a different extent; Similarly, *Dock3* and *Kcnt2* were up- and downregulated, respectively, in both Tat × Coc and Coc; *Yeats4* was upregulated in Tat × Coc but downregulated in Coc; and *Dcaf5* was upregulated in Tat × Coc but downregulated in Tat. In addition, genes *Itga3* in microglia and *Ank2* in astrocytes had an opposite direction of expression changes and offset each other in Tat × Coc factor; and genes *Col6a1* in microglia and *Tjp2* in astrocytes were either up- or downregulated in both Tat and Coc factors, indicating that they may have an additive effect between Tat and cocaine.

For CpH-related DMRs, there were 9,375 genes containing or proximal to Hyper-DMRs and 3,670 for Hypo-DMRs by Tat, and 631 genes were overlapped for both; for Coc, 5,379 genes were containing or proximal to Hyper-DMRs, 8,293 genes for Hypo-DMRs, and 822 genes for both; for Tat × Coc, 2,381 genes were containing or proximal to Hyper-DMRs, 3,188 genes for Hypo-DMRs, and 187 genes for both (Figure S5B; Table S6). In addition, there were 31, 35, and 14 Up-DEGs linked to Hypo-DMRs, and 62, 50, and 19 Down-DEGs linked to Hyper-DMRss by Tat, Coc, and Tat × Coc factors, respectively. Microglia was also most affected by all these factors, while the other five cell types showed similar effects among these three factors (Figure S5C). However, only a small number of genes were screened out for all three factors, which did not allow sufficient statistic power for further GO and KEGG enrichment analysis and volcano map and heatmap selection.

Cocaine exposure led to dendritic spine swelling without altering the number of neurons and neuronal branches in the presence of Tat

Based on the idea that genome-wide alteration could extensively affect cell morphology, we further investigated whether there are corresponding pathological changes of three major brain cells, neurons, microglia, and astrocytes, of iTat mice exposed to cocaine. In addition, to test whether there were brain region restrictions on pathological changes, we extended our observations from HIP to other two main brain regions, the cortex (CORT) and caudate putamen of dorsal striatum (CPU), which are also related to cognitive dysfunction. We first performed Golgi-Cox staining to determine morphological changes in neurons. Neurons

were characterized by spine density, average area, and length/width ratio, and quantitated by projecting stack images and modeling the spines.

In HIP (Figure 4A), iTat showed lower spine density than WT in all males. However, Coc showed higher spine density than Sal in all mice, and the effect was more pronounced in iTat 6m females than WT (left panel, Figure 4B). Coc showed higher spine average area than Sal in WT 6m males, iTat had smaller spine average area than WT in 6m females and higher spine average area than WT in 12m of both males and females exposed to Coc (middle panel, Figure 4B). Coc showed higher spine length/width ratio than Sal in WT 6m males, and iTat showed lower spine length/width ratio than WT in 6m females (right panel, Figure 4B). We also performed immunofluorescent staining against NeuN to determine the number of neurons (Figure S6A) using the number of DAPI+-stained cells as a reference. iTat showed lower NeuN+ cells/DAPI+ cells than WT in CA2 and CA3 regions (bracketed, Figure S6A) of all males and females of both 6m and 12m mice (Figure S6B). Similar trends of changes in spine morphology and the numbers of neurons were obtained in CORT (Figure S7; Table S3) and CPU (Figure S8; Table S3). Some notable differences included that generally larger dendritic spines in CORT and CPU made the differences more pronounced, that Tat-associated sparse and smaller dendritic spines in CORT was absent and to a lesser extent in CPU, and that even much thinner Tat-associated dendritic spines were found in CPU. Furthermore, we determined the length of neuronal branches, including dendrites and axons, and quantitated them by projecting stack images and segmenting the cell body (Figure S9A). In CORT, only iTat showed shorter branch length than WT in 6m males (Figure S9B). No significant differences in branch length were noted in HIP and CPU among all groups in our pilot study. These results together showed that iTat showed lower density of dendritic spines with shorter, wider, and smaller size morphology similar to the stubby shape (Risher et al., 2014), and Coc showed higher density with longer and thinner morphology similar to the filopodia or thin type (Risher et al., 2014), whereas iTat exposed to Coc showed higher density with shorter and bolder morphology close to the mushroom type but with a much larger size, indicating that cocaine exposure leads to dysgenesis-like dendritic spine swelling or synaptopathology.

Cocaine exposure led to significant increases of synaptophysin expression in the presence of Tat

We next performed western blotting to determine expression of two important neuronal functional markers post-synaptic density protein 95 (PSD-95) and pre-synaptic synaptophysin (SYP) in the brains of these mice (Figure 5A). In HIP, Coc showed lower PSD-95 expression than Sal in all groups, and iTat showed higher PSD-95 expression than WT in all Coc groups (Figure 5B). Coc showed significantly higher SYP expression than Sal in all groups except for 6m females, and iTat showed higher SYP expression than WT in all Coc groups. Similar trends were noted in both CORT (Figure S10A) and CPU (Figure S10B), although the differences were smaller in these two regions compared with HIP, and iTat showed higher PSD-95 and SYP than WT in 12m females. One consistent finding from all three brain regions was that Coc increased considerably more SYP expression in iTat mice than WT in all groups.

Cocaine exposure diminished microglia activation by Tat

We then performed immunohistochemistry staining for microglia marker Iba-1 and determined if there were changes in the number and morphology of microglia. The cell body and branches of Iba-1+ cells were segmented, and the branches were skeletonized. The branch length and endpoints were quantified for each individual cell. In HIP (Figure 6A), iTat had more microglia than WT in all groups except for 12m females (left panel, Figure 6B), and longer branch length (middle panel, Figure 6B) and more branch endpoints (right panel, Figure 6B) than WT in all groups. Coc had longer branch length and more branch endpoints than Sal in 6m of both males and females, while Coc had shorter branch length and fewer branch endpoints than Sal in iTat 6m of both males and females and iTat 12m males. The same findings were noted in CORT (Figure S11; Table S4) and CPU (Figure S12; Table S4), only differing in statistical significances. These results showed that Tat activated microglia to proliferate along with longer branches and more endpoints, Coc did not cause microglia to proliferate but with longer branches and more endpoints but, unexpectedly, Coc and Tat led to decreased branch length and endpoints of microglia while the higher number of microglia was maintained.

Cocaine exposure diminished astrocyte activation by Tat

We also performed immunohistochemistry staining for astrocyte marker glial fibrillary acidic protein (GFAP) and characterized the morphological changes of astrocytes in these mice. The cell body of GFAP + cells was segmented, and the total cell number and cell body occupied area were quantified. As astrocyte branches are thinner, more intercrossed, and denser than microglia, we first pronounced all the branches directly from images and then skeletonized them and quantified the total branch length in each view field. In the dentate gyrus of HIP (Figure 7A; Table S4), iTat had more astrocytes (left panel, Figure 7B), smaller cell body occupied area (middle panel, Figure 7B), and shorter branch length (right panel, Figure 7B) than WT in all groups. Except for branch length in both males and females of 12m, Coc showed smaller cell body occupied area and shorter branch length than Sal in all groups, except for branch length in 6m males, and showed even smaller cell body occupied area and shorter branch length than Sal in 6m iTat males, smaller cell body occupied area than Sal in 12m iTat females, and shorter branch lengths than Sal in 6m iTat females. There were very fewer astrocytes in CORT and CPU in GFAP staining and the changes in these cells were not very evident (Table S4, data not shown).

Age and sex had similarly independent contributions to pathological abnormalities by Tat and cocaine

Similar patterns of cellular response to Tat and cocaine were noted among all four groups of 2 ages × 2 sexes: 6m males, 6m females, 12m males, and 12m females (Tables S1, S3, and S4). In cellular response (Figure S13; Table S5), compared with 6m males/females, 12m males/females had fewer neurons in CORT but more microglia and astrocytes in HIP, CORT, and CPU, higher spine density in CORT, smaller spine average area in HIP, larger spine average area in CPU, higher spine length/width ratio in HIP, lower spine length/width ratio in CPU, higher PSD-95 level in spines in HIP, CORT, and CPU, lower SYP level in neuron axons in HIP and CORT, longer branches in neurons of CORT and astrocytes of

HIP astrocytes, shorter branches and fewer branch endpoints in microglia of HIP, CORT, and CPU, and larger cell body area in astrocytes of HIP. Males and females only differed in the distribution of statistical significance between these two age groups. Females had the statistical significance in CORT spine density, CPU spine average area, HIP spine length/width ratio, and HIP branch length of astrocytes, whereas males had the statistical significance in HIP spine average area, CPU spine length/width ratio, and CORT branch length of neurons.

In addition (Table S5), compared with males, females had fewer neurons in HIP, higher spine density, and spine average area in HIP and CORT, lower spine length/width ratio in HIP and CPU, higher PSD-95 level in HIP, CORT, and CPU, lower SYP level in CPU, longer branches in neurons of CORT, fewer microglia and shorter branch length and fewer branch endpoints in HIP and CPU, longer branch length and fewer branch endpoints in CORT, fewer astrocytes and shorter branch length in HIP. Both 6m and 12m mice mostly had the same response. 6m mice had statistical significance in spine length/width ratio in CPU, microglia counts in HIP with branch length and branch endpoints, which were not noted in 12m mice. Conversely, 12m mice had the statistical significance in spine density and spine average area in HIP, and microglia branch ending points in CORT, which were not noted in 6m mice. There were some exceptions; for example, neuron branch length in CORT, microglia branch ending points in CPU, and astrocyte branch length in HIP did not show the significance in both males and females, but only showed the significance in 6m mice that had opposite response compared with 12m mice.

DISCUSSION

Interactive effects between Tat and cocaine

Cocaine exerted its impact on the behaviors of iTat mice in an interactive manner and on glial and neuronal response by Tat in both interactive and additive manner (Table S8). Specifically, MWM indices with significant changes were all interactive effects (Tables S1 and S8). For morphological changes in neurons, SYP and PSD-95 expression levels had either interactive or additive effect, differing among the groups, and the spine morphology changes all showed interactive effects (Table S3 and S8). For morphological changes in microglia, all showed interactive effects, while, for morphological changes in astrocyte, all showed additive effects (Table S3 and S8). In agreement with our studies are other studies that show interactive or additive effects between cocaine and Tat, including cholesterol homeostasis of glia and neurons (Cotto et al., 2018b; Mohseni Ahooyi et al., 2018), excitability of pyramidal neurons in medial prefrontal cortex (Wayman et al., 2015), neuronal differentiation (Sun et al., 2016), brain energy metabolism (Natarajaseenivasan et al., 2018; Sivalingam et al., 2021), and addiction (McLaughlin et al., 2014). However, few of these studies have clearly clarified the differences between interactive and additive effects. Although both interactive and additive effects could lead to worse outcomes, the interactive effect is biologically more significant and often leads to more unpredictable outcomes.

In terms of neurobehaviors and neuropathology, Tat slightly impaired learning and memory (Figures 1B, 1C, and S1; Table S1) and altered spine morphology (Figures 4A, 4B, S7, and S8; Table S2). In contrast, cocaine showed better learning and memory, although there

was no statistical significance when compared with Sal. Cocaine was also associated with higher spine density, average area, and length/width ratio. However, Tat and cocaine together showed significantly worsened learning and memory and induced dramatic spine dysgenesis (swelling). Similarly, in HIP of 6m males and 12m females, Tat barely affected SYP expression, while cocaine increased SYP expression; However, Tat and cocaine together drastically elevated SYP expression (Figure 5; Table S2). For microglia morphology, Tat significantly increased branch length and number of branch endpoints, while cocaine had similar effects but to a much lesser extent. However, Tat and cocaine together led to remarkably decreased branch length and the branch endpoints (Figures 6, S11, and S12; Table S3). Furthermore, 14,838 Hyper- and 15,800 Hypo-CpG DMRs linked to 56 downregulated and 127 upregulated DEGs (Figures 2E and 3A), and 1,995 Hyper- and 2,762 Hypo-CpH DMRs linked to 19 downregulated and 14 upregulated DEGs (Figures S4E and S5B) were identified to be involved in the interactions between Tat and cocaine. All these findings strongly support the interactive nature between Tat and cocaine for the impact of cocaine in the HAND population.

Chronic cocaine use alone enhances spatial learning and memory (Del Olmo et al., 2007; Zhai et al., 2007), and spine density (Cahill et al., 2018; Norrholm et al., 2003; Shen et al., 2009), long-term potentiation in different brain regions (del Olmo et al., 2006; Fu et al., 2007; Overton et al., 1999), and altered spine morphology (Caffino et al., 2018; Rasakham et al., 2014). In this study, we show that changes of synaptic markers SYP and PSD-95 expression by cocaine varied among brain regions, age, and sex (Figures 5, S10, and S13; Table S2), indicating that effects of cocaine are context dependent. This possibility is supported by other behavioral findings in the study that cocaine unexpectedly and specifically showed somewhat anxiolytic effect on 6m females by EPM and OPT (Figures S2A and S2B; Table S8) and anti-depressive effect to 12m males by TST and FST (Figures S2D and S2E; Table S8). These findings are consistent with other studies (Ka et al., 2016; Ribeiro et al., 2017; Rodriguez-Espinosa and Fernandez-Espejo, 2015; Yao et al., 2004). Also, as demonstrated in other studies (Cotto et al., 2018a; Scofield et al., 2016), we showed that cocaine activated microglia in 6m mice with increased branch length and ending points and decreased astrocyte cell body regions and branch lengths (Figures 6, 7, S11, and S12; Table S3).

We and others have shown that Tat impairs spatial memory and locomotor activity (Zhao et al., 2020, 2021) and causes depressive status (Lawson et al., 2011; McLaughlin et al., 2017), neuronal cell loss (Jin et al., 2012; Zhou et al., 2004), shortened neuron dendrite branches (Rahimian and He, 2016), lower spine density (Fitting et al., 2010), and glia cells activation (Zhao et al., 2021; Zhou et al., 2004). These were confirmed in this study (Tables S1, S2, S3, S4, and S8). In the study, we also provide direct and *in vivo* evidence that Tat caused neuronal loss in HIP, CORT, and CPU, shortened neuron dendrite branches in CORT, lower spine density in HIP and CPU, microglia activation along with increased cell number and branches in HIP, CORT, and CPU, and astrocyte activation with increased cell number and decreased cell body and branch length in HIP. Furthermore, we showed mostly additive effects of age and sex in changes of behavioral and cellular responses to Tat and cocaine (Tables S1, S3, S4, S5, and S8), except that significant depressive status was noted in 6m males by FST and somewhat depressive status in 12m females by both TST and FST

(Figures S2D and S2E; Table S8), which indicates that age and sex function by different mechanisms. Another interesting new finding from this study is that all iTat mice showed higher anxious threshold (anxiolytic characteristic) in EPM and OPT even with cocaine (Figures S2A and S2B; Table S8). This could be altered locus coeruleus reactivity of the anxiety system by Tat (Morris et al., 2020) and merits further investigation.

Glial involvement in synaptic dysgenesis

We found that chronic cocaine use sharply diminished branch lengths of microglia and astrocytes along with synapse swelling in iTat mice (Figures 4, 6, 7, S7, S8, S11, and S12; Tables S3 and S4). A plausible explanation is that chronic cocaine use limits astrocyte-neuron contact and damages the microglia pruning process, which in turn leads to unrestrained synapse formation, resulting in synapse swelling or dysgenesis to have enough capacity to mediate impaired learning and memory processes (Figures 1B, 1C, and S1; Table S1). In addition, ECM, which constitutes around 20% brain volume, has been proposed to be a potential mediator for astrocyte-microglia-synapse interaction involved in synapse remodeling (Ferrer-Ferrer and Dityatev, 2018; Vainchtein and Molofsky, 2020). Our KEGG pathway analysis, which showed that the *ECM receptor interaction* pathway was significantly involved in Tat-, Coc-, and Tat/Coc-induced molecular changes in all three factors (Figure 3C), offers additional evidence to further support this possibility. Our GO functional analysis revealed that more neuron functional and morphological clusters were present under the Tat × Coc factor (Figure 3B), which could be the molecular basis for synaptic dysgenesis. Of note is that, although astrocytes play an important role during this process, the significant proportion of microglia-related genes with significant changes in their expression levels were identified in our bioinformatic analysis (Figure 3D). Finally, the morphology changes of microglia showed the interactive effect between Tat and Coc, which was different from additive effects in astrocytes (Table S8). All these findings support the notion that microglia is the major player during synaptic dysgenesis by Tat and Coc.

Roles of genome-wide DNA methylation by Tat and Coc

Most studies about cocaine-associated DNA methylation changes focus on the nucleus accumbens and prefrontal cortex of the brain and show different levels of genome-wide DNA methylation by different approaches (for review, see Brown and Feng, 2017). We have previously shown that Tat decreases genome-wide DNA methylation in CORT and cerebellum by ELISA (Zhao et al., 2020). In this study, we determined the genome-wide DNA methylation in HIP using single-base resolution WGBS. Tat or Tat and Coc decreased the CpG and CpH percentage, Coc had no significant changes in the CpG percentage and slight increases in the CpH percentage (Figures S14A and S14B), suggesting that Tat alters the mC sites and Coc does not. However, Tat increased the average methylation levels of each CpG and CpH site, and cocaine showed opposite effects (Figures 2A and S4A). Taken together, Tat reduced the numbers of CpG and CpH sites, but increased their average methylation level. In contrary, cocaine did not affect the numbers of CpG and CpH sites but decreased their average methylation level. These findings suggest that the changes at individual CpG and CpH site may be more valuable than the changes at the genome-wide level. In addition, we showed that the distribution of these mCpG and mCpH sites and their linked DMRs by Tat, Coc, or Tat and Coc did *not* show significant convergent effect

(Figures 2B-2E, S4B-S4E, and S5A), indicating that Tat and Coc hijack upstream genes/pathways that control DNA methylation. DNMT3B, which we identified to be responsive to Tat (Zhao et al., 2020), could be a strong candidate.

Tat as an accelerating factor of biological aging

In the study, we monitored body weights of all mice and found that iTat mice weighed significantly lower than WT mice in both 6m and 12m groups (Figure S15A), which extended our previous observation that there were weight differences between WT and iTat mice of 1 month (Kim et al., 2003). We also found that females weighed significantly lower than males in 6m iTat and WT mice as well as in 12m WT mice, but not in 12m iTat mice, suggesting that iTat mice could experience andropause and menopause earlier than WT mice or that their sex hormone could decline earlier than WT mice. In addition, we noticed that 12 m iTat mice had much higher mortality than 12m WT mice during cocaine injection (Table S9), although there was no statistical significance due to the small group number. Nonetheless, these results indicate that aging iTat mice are more vulnerable than WT mice to stress, such as injection, cocaine, or the declined adaptability of the cardiovascular system to stress earlier than WT mice. To ascertain this Tat aging connection (Zhao et al., 2020), we aligned HIP mC sites, which were generated from WGBS in 12m mice, with 732 documented age-related mC markers (Coninx et al., 2020). We identified 172 matched mC sites and found that the methylation level (M value) of 32 mC sites in iTat mice were significantly higher from WT mice (Figures S14C and S14D; Table S10). These results further demonstrated that iTat mice had higher biological age and support the idea that Tat accelerates biological aging.

Limitations of the study

There are several perceived limitations about this study. Use of iTat mice as a surrogate model for HAND could be one limitation. These mice only express HIV Tat protein and none of the other viral proteins, even though Tat is a major pathogenic factor for HAND. We also included MWM to determine memory changes of the mice in the context of Tat expression and Coc exposure. The results showed MWM to be the best neurobehavioral test among all other tests to demonstrate the interactive phenomenon between Tat and Coc. Stress and low sensitivity could affect the outcomes of MWM (Vorhees and Williams, 2014). Thus, alternative memory tests would further validate the findings. Based on the effects of Tat and Coc on the memory, we decided to choose the HIP region as our focus to determine the effects of Tat and Coc on DNA methylation and gene expression. Thus, it remains to be determined if similar changes occur in other brain regions, including CORT and CPU. Microglia, astrocytes, and neurons have been the main focus in the field of neuroHIV, as they represent the main targets of HIV infection and HIV-infected/affected cells. Our study shows significant changes of gene expression in oligodendrocytes and oligodendrocyte progenitor cells in response to Tat, Coc, and Tat × Coc. It would be interesting to determine the pathological changes, if any, in these cells exposed to Tat, Coc, and Tat × Coc. Finally, although we performed RNA-seq to confirm changes of gene expression, individual genes, and biological pathways in different cells identified from this study merit further investigation.

STAR ¦ METHODS

RESOURCE AVAILABILITY

Lead contact—Further information and requests for resources and reagents should be directed to and will be fulfilled by the Lead Contact, Johnny J. He (johnny.he@rosalindfranklin.edu).

Materials availability—This study did not generate new unique reagents.

Data and code availability

Data availability: All data reported in this paper will be shared by the lead contact upon request. The NGS data link is listed in the key resources table.

Code availability: This paper does not report original code.

Any additional information that may be required to reanalyze the data reported in this paper is available from the lead contact upon request.

EXPERIMENTAL MODEL AND SUBJECT DETAILS

Mice and cocaine administration—Wild-type (Wt, C57BL/6) mice were purchased from Jackson Laboratory (Bar Harbor, ME), and iTat mice were created as we described before (Kim et al., 2003). All the animal procedures were approved by the Institutional Animal Care and Use Committee. Mice were housed with a 12-h light and 12-h dark photoperiod and provided water and food *ad libitum*. Mice were fed with Dox food pellets, beginning at day 21 following their weaning and continued for 5 or 11 months, then *i*.p. injected with cocaine (Coc, 30 mg/kg/day, stock: 3 mg/mL) or its solvent saline (Sal) for 14 days. These mice remained on Dox food pellets throughout the Coc injection and behavioral assessments until they were euthanized. Eventually, all mice were fed for a total of either 6.5- or 12.5-month, which were designated as 6m or 12m throughout the study for simplicity. There were a total of 194 mice in the study, which were randomly assigned (10–16 mice/group) to 16 experimental groups [2 genotypes (Wt, iTat) x 2 sexes (male, female) x 2 age groups (6m, 12m) x 2 treatments (Sal, Coc). For all experimental groups, an equal number of age-matched male and female mice were included.

METHOD DETAILS

Behavioral tests—10 days after final injection (drug free/cessation period), All mice remained drug free for 10 days and then subjected to before behavioral battery tests in the order of increasing stress. ***Elevated plus maze (EPM) test***: In the low light intensity environment, mouse was placed in the central area of EPM apparatus, faced to open arm, and allowed travel freely between open arms and close arms for five minutes. Then, their travel distance, staying time, and entries in each area/arm were monitored by an infrared camera, and Open Arm Entries, Open Arm Time, and Open Arm Distance were finally used for measuring the anxious status. ***Open field test (OPT)***: Mice were allowed to move freely in an acrylic chamber, for 10 min, and the Total Distance, Maximum Speed, Central Distance (in the middle square area with 20 cm × 20 cm size), and Central Entries during the

movement were recorded for analyzing its locomotor activity and anxious status. ***Rotarod test (RT)***: There are two sessions in two days for RT. Sensitive speed screening session (Day 1): In this session, there were total four trials for each mouse, and the interval between each trial was around 15 min, but no more than 20 min. Mice were first placed on the stationary rod of IITC Rotarod for 30 s, then started with the acceleration mode from 4 to 45 rpm within 4 min. The speed at which the mouse fell from rod was record, and the average falling-down speed for four trails was calculated. We noted that most young mice fell at 20–35 rpm, and most old mice at 10–20 rpm. So, 30 rpm and 15 rpm were chosen as the sensitive speed for young and old mice, respectively. For the second session test (Day 2), there were two trials for each mouse, and every trial had 4 min test with a fixed sensitive speed (fixed mode). Similarly, mice were placed on the stationary rod for 30 s, then started with their sensitive speed. The latency to fall from the rod was record. ***Morris water maze test (MWM)***: The apparatus and protocol were as previously described (Zhao et al., 2021), except that we added to another probe test seven days after first probe test to measure the long-term memory. Briefly, there were two stages including 5-day training and two probe tests. Training stage consisted of four trials. In each trial, mice were put into one quadrant and allowed to freely seek the platform within 90 s. If they found the platform within 90 s, they would be allowed to stay on the platform for another 10 s for memorizing purpose. However, if they failed, they would be put onto the platform to stay for 15 s. Immobile or floating Mice were excluded from the experiments. First probe test was implemented on the next day after the 5-day training stage with a 60 s trial, and the second probe test was the same as the first one, but was carried out seven days later. The platform was removed during the probe tests. One day after second probe test, mice were euthanized and the brains were collected. All behavioral tests were record and analyzed by a computerized video tracking system, Anymaze.

DNA and RNA isolation, library preparation, and sequencing—Genomic DNA was isolated from one HIP hemisphere by DNeasy Blood & Tissue Kit, the DNA quality was first confirmed by Nanodrop, with 260/280 ratio at 1.95–2.0 (in 10 mM Tris·Cl, pH 7.5 solution) and then verified by 1% agarose gel analysis to make sure no DNA degradation and RNA contamination. Genomic DNA libraries were prepared genomic DNA (10 ng) using a Pico Methyl-Seq Library Prep Kit. MQ beads, were used in place of the column purification system in the library kit for higher DNA recovery. The quality of DNA libraries was determined to be 380–520 bp of the median size and have no contamination of primer dimers. The libraries were sequenced using the Illumina NovaSeq 6000 S4 Paired-end-150 system. RNA was isolated from the other HIP hemisphere of the same mice by TRIzol reagent, and further purified using an RNA Clean & Concentrator Kit. The RNA was determined to be 9.5–9.9 of RNA integrity number using an Agilent Bioanalyzer 2100. The RNA libraries were prepared from the RNA using a QIAseq Stranded mRNA Select kit. Briefly, RNA (800 ng) was used to generate poly-A+ enriched RNA, the concentration of which was determined using a Qubit 4 Fluorometer. poly-A+ enriched RNA (10 ng) was used to synthesize the RNA libraries using the kit. The quality of libraries was determined to be 300–500 bp of the median size and have no contamination of primer dimers using a bioanalyzer. The libraries were sequenced using the Illumina HiSeq 4000 Single-end-50 system.

Sequencing data processing and analysis—A bioinformatics analysis pipeline nf-core/methylseq (Ewels et al., 2020) was used to process the methylation (Bisulfite) sequencing data. Briefly, we input the FASTQ raw data, aligned the reads, and performed extensive quality-control on the results. In the pipeline, FASTQC (v 0.11.9) was chosen for quality control and Trim Galore! (v0.6.5) for adapter sequence trimming with default parameters. Trimmed sequences were then mapped to the Mus musculus assembly (GRCm38/mm10) from Genome Reference Consortium, using Bismark 0.22.3 (Krueger and Andrews, 2011) with the alignment tool Bowtie2 (v2.4.2) (Langmead and Salzberg, 2012). Sequence duplicates were further removed by command “deduplicate_bismark” and context-dependent methylation (CpG and CpH) were extracted by command “bismark_methylation_extractor”.

Differential methylation calculation—M-value was used as metrics to measure methylation levels and differential analysis of methylation levels, which was defined as the log2 ratio of the intensities of methylated probe versus unmethylated probe as followed (Du et al., 2010):

$$M = log\,2\left(\frac{m+\alpha}{\mu+\alpha}\right), \quad \text{(Equation 1)}$$

where m and μ are methylated and unmethylated level, respectively, measured by the methylated and unmethylated probes for an interrogated CpG site respectively, and α is a constant offset and set as 1e-3. We modeled each CpG or CpH site once for differential methylation analysis. For each site and preset region, we considered the following linear mixed model to determine differential methylation:

$$M_{ijk} = \mu + S_i + P_j + T_k + PT_{jk} + SP_{ij} + ST_{ik} + \varepsilon_{ijk}, \quad \text{(Equation 2)}$$

where $\varepsilon_{ijk} \sim N(0,\sigma^2)$. The fixed effects in equation are μ (mean), S_i (sex, male or female), P_j (genotype, iTat or Wt), T_k (treatment, Coc or Sal), PT_{jk} (genotype-treatment interaction), SP_{ij} (sex-genotype interaction), and ST_{ik} (sex-treatment interaction); i = 1,2 stands for male and female, respectively; j = 1,2 stands for iTat and Wt mice, respectively; and k = 1,2 stands for Coc and Sal treatment, respectively. The variance components in the linear mixed model were estimated using the residual maximum likelihood (REML) approach (Pinheiro and Bates, 2002). We used R program to fit linear mixed models to each site and preset region. The lsmeans package was used for testing the differences in combinations of levels among genotype and treatment, and for tests of Difference-in-Differences in the interaction between genotype and treatment. Initially, we performed the Principal component analysis (PCA) analyses using the built-in R functions prcomp() and found there were no significant difference by sex factor (Figure S3B). We then only considered two factors, genotype and treatment, and defined the vectors with only four values [Wt mice with Sal (Wt-Sal), iTat mice with Sal (iTat-Sal), Wt mice with Coc (Wt-Coc), and iTat mice with Coc (iTat-Coc)] to represent the means we used to compare. Thereafter, we built the custom comparisons via the Contrast () function in lsmeans package. For example, Wt-Coc vs. Wt-Sal is defined as (0, 1, 0, −1), iTat-Sal vs. Wt-Sal as (0, 0, 1, −1), and interaction between type (iTat/Wt) and treatment (Coc/Sal) as (1, −1, −1, 1).

Annotation with custom regions—Our preset regions were downloaded from annotatr package (Cavalcante and Sartor, 2017), which provides genomic annotations including 1 to 5 kb, promoters, 3UTRs, 5UTRs, exons, exon boundaries, introns, and intergenic. Then, three critical regions, including promotors, exons, and introns were parsed and merged with GRCm38 gene annotation file for region analysis.

RNA sequencing (RNA-Seq) data processing—Reads were mapped to GRCm38 reference genomes with STAR (v2.7.9) (Dobin et al., 2013). The maximum number of multiple alignments allowed for a read is set to 10. And, featureCounts (v 2.0.1.13) was used to quantify reads with the following parameters (-T 10 -t exon -s 1 -g exon_id). The read count matrix was then normalized by countToFPKM package (v 1.0) to Fragments Per Kilobase of transcript per Million mapped reads (FPKM) values. For each exon, we applied the quantified expression value Y_{ijk} the same linear mixed model as shown in Equation 2 to determine differential expression:

$$Y_{ijk} + \mu + S_i + P_j + T_k + PT_{jk} + SP_{ij} + ST_{ik} + \varepsilon_{ijk}, \quad \text{(Equation 3)}$$

where variables and subscripts are same as Equation 2, except for Y_{ijk} which is a quantified expression value. A PCA analysis were performed and found there were no significant difference by sex factor (Figure S3B).

Gene-linked DMR—To determine the potential genes which were possibly regulated by differentially methylated regions (DMR). We defined Gene-linked DMR as the differentially methylated regions mapped to or close to genes that are differentially expressed (DEG) in RNA-Seq. Gene expression values were measured at the exon level from RNA-Seq by feature Counts, in order to increase mapping with DMR. We merged the DMR annotated from annotatr package (Cavalcante and Sartor, 2017) and differentially expressed exons from RNA-Seq by transcript ID. There were totally four types of gene-linked DMR: Hyper-methylated DMR (Hyper-DMR) linked to up-regulated genes (Up-DEG), Hyper-DMR linked to down-regulated genes (Down-DEG), Hypo-methylated DMR (Hypo-DMR) linked to Up-DEG, and Hypo-DMR linked to Down-DEG. Only Hyper-DMR linked to Down-DEG and Hypo-DMR linked to Up-DEG were used for down-stream analysis.

KEGG and gene ontology analysis—We performed pathway analysis through the Database for Annotation, Visualization and Integrated Discovery (DAVID) v6.8 (Huang et al., 2009). Functional Annotation Table for the three factors, Tat, Coc, and Tat X Coc, was downloaded through the DAVID API Server.

Machine learning for cell type prediction—In order to predict the cell types for gene-linked DMR, we first downloaded the top 6000 ranked cell type-enriched mouse genes from the reference (McKenzie et al., 2018) and mapped them with the RNA-Seq transcriptome database of purified cell classes of the brain (Zhang et al., 2014). The Support Vector Machine (Zhang et al., 2021) was used to build a learning model from the mapped genes, and then the trained model was applied to predict the cell type for the unmapped genes and generated a database with cell type information. The following parameters were used for training: method = “C-classification”, kernel = “radial”, scale = TRUE, gamma = 1, and

cost = 1000. “Astro.1”, “Astro.2”, “Neuron.1”, “Neuron.2”, “OPC.1”, “OPC.2”, “NFO.1”, “NFO.2”, “Myelinating.1”, “Myelinating.2”, “MGL1”, “MGL2”, “Endo.1”, “Endo.2” were used for features. An internal five-fold cross-validation method evaluated that its prediction accuracy could reach 80%. Finally, we mapped the gene-linked DMR to this database. Finally, we mapped the gene-linked DMR to this database.

Golgi-Cox staining—After the mice were euthanized, the brain was extracted and sagittally dissected into two hemispheres. Golgi-Cox staining was performed as described (Zaqout and Kaindl, 2016). Briefly, one hemisphere was fixed in the Golgi-Cox solution at room temperature for 24 h and in the fresh Golgi-Cox solution for 10 more days. The tissue was then dehydrated and preserved in tissue-protectant solution at 4°C for 24 h and in the fresh tissue-protectant solution for seven more days. All these procedures were performed in dark. The tissue was then sagittally sectioned on a vibratome (100 μm thick, Leica, VT1000S). The sections were developed in ammonia solution (3:1) and 5% sodium thiosulfate solution, dehydrated in gradient ethanol and then in xylene, and mounted. All dendritic spine stack images were taken using a Nikon Eclipse 800 microscope with a 100x oil objective, while a 20x objective was used for neuronal branches stack images.

3′-Diaminobenzidine (DAB) staining—DAB staining was performed as we described (Zhao et al., 2021). Briefly, mice were anesthetized by avertin (tribromoethanol) and transcardially perfused with phosphate-buffered saline (PBS) and then 4% paraformaldehyde (PFA). The brains were dissected out, fixed, dehydrated, embedded, and sagittally sectioned with a cryostat (20 μm thick). Floating sections were permeabilized, blocked, probed by Iba-1 antibody or GFAP antibody, inactivated endogenous peroxidases, probed again by a goat anti-rabbit secondary antibody, and developed using a DAB kit. All images were taken using a Nikon Eclipse E800 microscope with a 20x objective for iba-1 staining and 40x for GFAP staining.

Immunofluorescence staining—Brain sections (20 μm thick) were permeabilized, blocked, probed by NeuN and secondary antibody goat anti-mouse 488, and counter stained in 1 μg/mL DAPI. All images were taken using a Nikon Eclipse E800 microscope with a 10x objective.

Western blotting—Different brain regions, including hippocampus (HIP), caudate putamen (CPU), and cortex (CORT), were dissected out from the fresh frozen brains at −80°C, placed in RIPA buffer (50 mM Tris.HCl, pH 8.0, 280 mM NaCl, 0.5% NP-40, 1% C24H39NaO4, 0.2 mM EDTA, 2 mM EGTA and 10% glycerol) supplemented with protease inhibitors, and briefly sonicated on ice to obtain the lysates. Protein concentrations of the lysates were determined using a Bio-Rad DC protein assay kit, the lysates were denatured in the SDS-PAGE loading buffer at 100°C for 10 min, electrophoretically separated by 8–10% SDS-PAGE, transfer onto 0.45 μm polyvinylidene fluoride membrane, and probed using appropriate antibodies against PSD-95, synaptophysin, and β-actin. A Bio-Rad ChemicDoc imaging system was used to capture images.

QUANTIFICATION AND STATISTICAL ANALYSIS

Image analysis—*For dendritic spine morphology from Golgi staining*: All z stack images were firstly projected into 2D images by image J (Schneider et al., 2012) with EDF plugin (Forster et al., 2004), then input to Imaris software (Bitplane) to analyze Spine Density, Spine Average Area, and Spine Length/Width ratio. All spine were chosen from the terminal branches of neuron dendrites with at least 60 μm in length, every dendritic branch was selected from a different individual neuron, three to four neurons were picked up from each section, three sections were selected from each individual mouse, every experimental group had three mice, and finally 9–12 spines were allocated to each group for statistical analysis. In HIP, only CA regions were included for analysis; in CORT, dendritic branches were randomly chosen from frontal, occipital, and parietal cortex, but every region had at least one dendritic branch; and in CPU, random dendritic branches were selected, as neuron morphology in this region was more uniform. ***For neuronal branches from Golgi staining***: All z stack images were projected into 2D images first, then input to ilastik (Berg et al., 2019) to run the cell body and branch segmentation, and lastly, analyzed by Cellprofiler (McQuin et al., 2018). Only the CORT region was selected for this analysis, as no apparent changes were observed in HIP and CPU in our pilot study. ***For microglia morphology from Iba-1 DAB staining***: All branches of microglia were pronounced by ilastik and analyzed by Cellprofiler. ***For astrocyte morphology from GFAP DAB staining***: Image J was used to segment the cell body region and count the cell number; and astrocyte branches were pronounced by ilastik and calculated by Cellprofiler. We only chose HIP dentate gyrus (DG) region in this analysis because of its significance as well as most if not all negative GFAP staining in CORT and CPU regions. ***For neuron number from NeuN immunofluorescence staining***: In HIP, only a specific area located at CA2-CA3 region (framed by white box in Figure 2C) was chosen for analysis; the green (NeuN+) and blue (DAPI+) channels in this area were split by image J, then the cell body signals in green channel were pronounced by ilastik and calculated by Cellprofiler. The blue channel in HIP and all staining signals in CORT and CPU regions were directly processed by Cellprofiler. In HIP and CPU, three random areas were chosen from each section; in CORT, three areas were chosen for each of frontal, occipital and parietal cortex from each section, thus three areas from three cortex regions were averaged for CORT analysis; for all the brain regions, three to five sections were selected from each mouse, every group had three mice, and there were 9–15 sections for each group for statistical analysis.

Statistical analysis—Four-way repeated measures ANOVA was used in MWZ training stages, and all other studies used either two-way or four-way ANOVA, whenever applicable; Bonferroni test was used for all post hoc analyses. All statistical analyses were performed using the IBM SPSS 20; and $p < 0.05$ was considered significant and marked as *, # or $ for comparisons among different groups; $p < 0.01$ and $p < 0.001$ were both considered highly significant and marked as ** and ***, respectively. For all bioinformatic data analysis, R program with $q < 0.05$ or $p < 0.05$ was used, and other details were provided the sections above. Interactive effect between Tat and cocaine was defined by ANOVA tests or Linear mix model analysis. If there was no interactive effect and combined effect of these two factors was more than each of the factors alone, it was defined as additive effect.

Supplementary Material

Refer to Web version on PubMed Central for supplementary material.

ACKNOWLEDGMENTS

This work was supported in part by grants R01DA043162 and R01NS094108 (to J.J.H.) and P20GM103449 from the National Institutes of Health, United States.

INCLUSION AND DIVERSITY

We worked to ensure sex balance in the selection of non-human subjects. We worked to ensure diversity in experimental samples through the selection of the cell lines. We worked to ensure diversity in experimental samples through the selection of the genomic datasets.

REFERENCES

Baldwin GC, Tashkin DP, Buckley DM, Park AN, Dubinett SM, and Roth MD (1997). Marijuana and cocaine impair alveolar macrophage function and cytokine production. Am. J. Respir. Crit. Care Med 156, 1606–1613. 10.1164/ajrccm.156.5.9704146. [PubMed: 9372683]

Berg S, Kutra D, Kroeger T, Straehle CN, Kausler BX, Haubold C, Schiegg M, Ales J, Beier T, Rudy M, et al. (2019). ilastik: interactive machine learning for (bio)image analysis. Nat. Methods 16, 1226–1232. 10.1038/s41592-019-0582-9. [PubMed: 31570887]

Brown AN, and Feng J (2017). Drug addiction and DNA modifications. Adv. Exp. Med. Biol 978, 105–125. 10.1007/978-3-319-53889-1_6. [PubMed: 28523543]

Caffino L, Messa G, and Fumagalli F (2018). A single cocaine administration alters dendritic spine morphology and impairs glutamate receptor synaptic retention in the medial prefrontal cortex of adolescent rats. Neuropharmacology 140, 209–216. 10.1016/j.neuropharm.2018.08.006. [PubMed: 30092246]

Cahill ME, Walker DM, Gancarz AM, Wang ZJ, Lardner CK, Bagot RC, Neve RL, Dietz DM, and Nestler EJ (2018). The dendritic spine morphogenic effects of repeated cocaine use occur through the regulation of serum response factor signaling. Mol. Psychiatry 23, 1474–1486. 10.1038/mp.2017.116. [PubMed: 28555077]

Cavalcante RG, and Sartor MA (2017). annotatr: genomic regions in context. Bioinformatics 33, 2381–2383. 10.1093/bioinformat-ics/btx183. [PubMed: 28369316]

Clark KH, Wiley CA, and Bradberry CW (2013). Psychostimulant abuse and neuroinflammation: emerging evidence of their interconnection. Neurotox. Res 23, 174–188. 10.1007/s12640-012-9334-7. [PubMed: 22714667]

Coninx E, Chew YC, Yang X, Guo W, Coolkens A, Baatout S, Moons L, Verslegers M, and Quintens R (2020). Hippocampal and cortical tissue-specific epigenetic clocks indicate an increased epigenetic age in a mouse model for Alzheimer's disease. Aging (Albany NY) 12, 20817–20834. 10.18632/aging.104056. [PubMed: 33082299]

Cotto B, Li H, Tuma RF, Ward SJ, and Langford D (2018a). Cocaine-mediated activation of microglia and microglial MeCP2 and BDNF production. Neurobiol. Dis 117, 28–41 10.1016/j.nbd.2018.05.017. [PubMed: 29859319]

Cotto B, Natarajaseenivasan K, Ferrero K, Wesley L, Sayre M, and Langford D (2018b). Cocaine and HIV-1 Tat disrupt cholesterol homeostasis in astrocytes: implications for HIV-associated neurocognitive disorders in cocaine user patients. Glia 66, 889–902. 10.1002/glia.23291. [PubMed: 29330881]

Cross SH, Lee M, Clark VH, Craig JM, Bird AP, and Bickmore WA (1997). The chromosomal distribution of CpG islands in the mouse: evidence for genome scrambling in the rodent lineage. Genomics 40, 454–461. 10.1006/geno.1996.4598. [PubMed: 9073513]

Del Olmo N, Higuera-Matas A, Miguéns M, García-Lecumberri C, and Ambrosio E (2007). Cocaine self-administration improves performance in a highly demanding water maze task. Psychopharmacology (Berl) 195, 19–25. 10.1007/s00213-007-0873-1. [PubMed: 17641875]

del Olmo N, Miguéns M, Higuera-Matas A, Torres I, García-Lecumberri C, Solís JM, and Ambrosio E (2006). Enhancement of hippocampal long-term potentiation induced by cocaine self-administration is maintained during the extinction of this behavior. Brain Res. 1116, 120–126. 10.1016/j.brainres.2006.07.001. [PubMed: 16979145]

Dobin A, Davis CA, Schlesinger F, Drenkow J, Zaleski C, Jha S, Batut P, Chaisson M, and Gingeras TR (2013). STAR: ultrafast universal RNA-seq aligner. Bioinformatics 29, 15–21. 10.1093/bioinformatics/bts635. [PubMed: 23104886]

Du P, Zhang X, Huang CC, Jafari N, Kibbe WA, Hou L, and Lin SM (2010). Comparison of Beta-value and M-value methods for quantifying methylation levels by microarray analysis. BMC Bioinformatics 11, 587. 10.1186/1471-2105-11-587. [PubMed: 21118553]

Egger M, May M, Chêne G, Phillips AN, Ledergerber B, Dabis F, Costagliola D, D'Arminio Monforte A, de Wolf F, Reiss P, et al. (2002). Prognosis of HIV-1-infected patients starting highly active antiretroviral therapy: a collaborative analysis of prospective studies. Lancet 360, 119–129. 10.1016/s0140-6736(02)09411-4. [PubMed: 12126821]

Ewels PA, Peltzer A, Fillinger S, Patel H, Alneberg J, Wilm A, García MU, Di Tommaso P, and Nahnsen S (2020). The nf-core framework for community-curated bioinformatics pipelines. Nat. Biotechnol 38, 276–278. 10.1038/s41587-020-0439-x. [PubMed: 32055031]

Ferrer-Ferrer M, and Dityatev A (2018). Shaping synapses by the neural extracellular matrix. Front. Neuroanat 12, 40. 10.3389/fnana.2018.00040. [PubMed: 29867379]

Fitting S, Xu R, Bull C, Buch SK, El-Hage N, Nath A, Knapp PE, and Hauser KF (2010). Interactive comorbidity between opioid drug abuse and HIV-1 Tat: chronic exposure augments spine loss and sublethal dendritic pathology in striatal neurons. Am. J. Pathol 177, 1397–1410. 10.2353/ajpath.2010.090945. [PubMed: 20651230]

Forster B, Van De Ville D, Berent J, Sage D, and Unser M (2004). Complex wavelets for extended depth-of-field: a new method for the fusion of multichannel microscopy images. Microsc. Res. Tech 65, 33–42. 10.1002/jemt.20092. [PubMed: 15570586]

Fox HC, D'Sa C, Kimmerling A, Siedlarz KM, Tuit KL, Stowe R, and Sinha R (2012). Immune system inflammation in cocaine dependent individuals: implications for medications development. Hum. Psychopharmacol 27, 156–166. 10.1002/hup.1251. [PubMed: 22389080]

Fu Y, Pollandt S, Liu J, Krishnan B, Genzer K, Orozco-Cabal L, Gallagher JP, and Shinnick-Gallagher P (2007). Long-term potentiation (LTP) in the central amygdala (CeA) is enhanced after prolonged withdrawal from chronic cocaine and requires CRF1 receptors. J. Neurophysiol 97, 937–941. 10.1152/jn.00349.2006. [PubMed: 17079348]

Gandhi N, Saiyed ZM, Napuri J, Samikkannu T, Reddy PV, Agudelo M, Khatavkar P, Saxena SK, and Nair MP (2010). Interactive role of human immunodeficiency virus type 1 (HIV-1) clade-specific Tat protein and cocaine in blood-brain barrier dysfunction: implications for HIV-1-associated neurocognitive disorder. J. Neurovirol 16, 294–305. 10.3109/13550284.2010.499891. [PubMed: 20624003]

Henderson LJ, Johnson TP, Smith BR, Reoma LB, Santamaria UA, Bachani M, Demarino C, Barclay RA, Snow J, Sacktor N, et al. (2019). Presence of Tat and transactivation response element in spinal fluid despite antiretroviral therapy. AIDS 33, S145–S157. 10.1097/QAD.0000000000002268. [PubMed: 31789815]

Huang DW, Sherman BT, and Lempicki RA (2009). Systematic and integrative analysis of large gene lists using DAVID bioinformatics resources. Nat. Protoc 4, 44–57. 10.1038/nprot.2008.211. [PubMed: 19131956]

Hudson L, Liu J, Nath A, Jones M, Raghavan R, Narayan O, Male D, and Everall I (2000). Detection of the human immunodeficiency virus regulatory protein tat in CNS tissues. J. Neurovirol 6, 145–155. 10.3109/13550280009013158. [PubMed: 10822328]

Jin J, Lam L, Sadic E, Fernandez F, Tan J, and Giunta B (2012). HIV-1 Tat-induced microglial activation and neuronal damage is inhibited via CD45 modulation: a potential new treatment target for HAND. Am. J. Transl. Res 4, 302–315. [PubMed: 22937208]

Johnson TP, Patel K, Johnson KR, Maric D, Calabresi PA, Hasbun R, and Nath A (2013). Induction of IL-17 and nonclassical T-cell activation by HIV-Tat protein. Proc. Natl. Acad. Sci. U S A 110, 13588–13593. 10.1073/pnas.1308673110. [PubMed: 23898208]

Jones M, Olafson K, Del Bigio MR, Peeling J, and Nath A (1998). Intraventricular injection of human immunodeficiency virus type 1 (HIV-1) tat protein causes inflammation, gliosis, apoptosis, and ventricular enlargement. J. Neuropathol. Exp. Neurol 57, 563–570. [PubMed: 9630236]

Jonkman S, and Kenny PJ (2013). Molecular, cellular, and structural mechanisms of cocaine addiction: a key role for microRNAs. Neuropsychopharmacology 38, 198–211. 10.1038/npp.2012.120. [PubMed: 22968819]

Ka M, Kook YH, Liao K, Buch S, and Kim WY (2016). Transactivation of TrkB by Sigma-1 receptor mediates cocaine-induced changes in dendritic spine density and morphology in hippocampal and cortical neurons. Cell Death Dis. 7, e2414. 10.1038/cddis.2016.319. [PubMed: 27735948]

Kim BO, Liu Y, Ruan Y, Xu ZC, Schantz L, and He JJ (2003). Neuropathologies in transgenic mice expressing human immunodeficiency virus type 1 Tat protein under the regulation of the astrocyte-specific glial fibrillary acidic protein promoter and doxycycline. Am. J. Pathol 162, 1693–1707. 10.1016/S0002-9440(10)64304-0. [PubMed: 12707054]

Klein TW, Matsui K, Newton CA, Young J, Widen RE, and Friedman H (1993). Cocaine suppresses proliferation of phytohemagglutinin-activated human peripheral blood T-cells. Int. J. Immunopharmacol 15, 77–86. 10.1016/0192-0561(93)90033-u. [PubMed: 8432625]

Kousik SM, Napier TC, and Carvey PM (2012). The effects of psychostimulant drugs on blood brain barrier function and neuroinflammation. Front. Pharmacol 3, 121.10.3389/fphar.2012.00121. [PubMed: 22754527]

Krueger F, and Andrews SR (2011). Bismark: a flexible aligner and methylation caller for Bisulfite-Seq applications. Bioinformatics 27, 1571–1572. 10.1093/bioinformatics/btr167. [PubMed: 21493656]

Kumar S, Rao PS, Earla R, and Kumar A (2015). Drug-drug interactions between anti-retroviral therapies and drugs of abuse in HIV systems. Expert Opin. Drug Metab. Toxicol 11, 343–355. 10.1517/17425255.2015.996546. [PubMed: 25539046]

Langmead B, and Salzberg SL (2012). Fast gapped-read alignment with Bowtie 2. Nat. Methods 9, 357–359. 10.1038/nmeth.1923. [PubMed: 22388286]

Lawson MA, Kelley KW, and Dantzer R (2011). Intracerebroventricular administration of HIV-1 Tat induces brain cytokine and indoleamine 2,3-dioxygenase expression: a possible mechanism for AIDS comorbid depression. Brain Behav. Immun 25, 1569–1575. 10.1016/j.bbi.2011.05.006. [PubMed: 21620953]

Liao Y, Smyth GK, and Shi W (2014). featureCounts: an efficient general purpose program for assigning sequence reads to genomic features. Bioinformatics 30, 923–930. 10.1093/bioinformatics/btt656. [PubMed: 24227677]

Litvin PY, Siders CA, Waite EN, Woo E, Romero E, Foley J, Ettenhofer ML, Gooding AL, Castellon S, Hinkin C, and Wright MJ (2019). Recent cocaine use and memory impairment in HIV. Appl. Neuropsychol. Adult, 1–12. 10.1080/23279095.2019.1683562.

Martin E, Keutmann MK, Fogel JS, Maki PM, Gonzalez R, Vassileva J, Rubin LH, and Hardy D (2018). Verbal and spatial working memory among drug-using HIV-infected men and women. J. Neurovirol 24, 488–497. 10.1007/s13365-018-0639-z. [PubMed: 29687402]

May SB, Barroso PF, Nunes EP, Barcaui HS, Almeida MM, Costa MD, Faulhaber JC, Santoro-Lopes G, and Schechter M (2007). Effectiveness of highly active antiretroviral therapy using non-brand name drugs in Brazil. Braz. J. Med. Biol. Res 40, 551–555. 10.1590/s0100-879x2007000400014. [PubMed: 17401499]

McKenzie AT, Wang M, Hauberg ME, Fullard JF, Kozlenkov A, Keenan A, Hurd YL, Dracheva S, Casaccia P, Roussos P, and Zhang B (2018). Brain cell type specific gene expression and co-expression network architectures. Sci. Rep 8, 8868. 10.1038/s41598-018-27293-5. [PubMed: 29892006]

McLaughlin JP, Ganno ML, Eans SO, Mizrachi E, and Paris JJ (2014). HIV-1 Tat protein exposure potentiates ethanol reward and reinstates extin-guished ethanol-conditioned place preference. Curr. HIV Res 12, 415–423. 10.2174/1570162x1206150311160133. [PubMed: 25760047]

McLaughlin JP, Paris JJ, Mintzopoulos D, Hymel KA, Kim JK, Cirino TJ, Gillis TE, Eans SO, Vitaliano GD, Medina JM, et al. (2017). Conditional human immunodeficiency virus transactivator of transcription protein expression induces depression-like effects and oxidative stress. Biol. Psychiatry Cogn. Neurosci. Neuroimaging 2, 599–609. 10.1016/j.bpsc.2017.04.002. [PubMed: 29057370]

McQuin C, Goodman A, Chernyshev V, Kamentsky L, Cimini BA, Karhohs KW, Doan M, Ding L, Rafelski SM, Thirstrup D, et al. (2018). Cell-Profiler 3.0: next-generation image processing for biology. PLoS Biol. 16, e2005970. 10.1371/journal.pbio.2005970. [PubMed: 29969450]

Meade CS, Addicott M, Hobkirk AL, Towe SL, Chen NK, Sridharan S, and Huettel SA (2018). Cocaine and HIV are independently associated with neural activation in response to gain and loss valuation during economic risky choice. Addict. Biol 23, 796–809. 10.1111/adb.12529. [PubMed: 28682013]

Meyer VJ, Little DM, Fitzgerald DA, Sundermann EE, Rubin LH, Martin EM, Weber KM, Cohen MH, and Maki PM (2014). Crack cocaine use impairs anterior cingulate and prefrontal cortex function in women with HIV infection. J. Neurovirol 20, 352–361. 10.1007/s13365-014-0250-x. [PubMed: 24760360]

Mohseni Ahooyi T, Shekarabi M, Torkzaban B, Langford TD, Burdo TH, Gordon J, Datta PK, Amini S, and Khalili K (2018). Dysregulation of neuronal cholesterol homeostasis upon exposure to HIV-1 tat and cocaine revealed by RNA-sequencing. Sci. Rep 8, 16300. 10.1038/s41598-018-34539-9. [PubMed: 30390000]

Moreno A, Perez-Elías MJ, Casado JL, Muñoz V, Antela A, Dronda F, Navas E, Fortún J, Quereda C, and Moreno S (2000). Effectiveness and pitfalls of initial highly active antiretroviral therapy in HIV-infected patients in routine clinical practice. Antivir. Ther 5, 243–248. [PubMed: 11142618]

Morrell JI, Basso JC, and Pereira M (2011). Both high and low doses of cocaine derail normal maternal caregiving - lessons from the laboratory rat. Front. Psychiatry 2, 30. 10.3389/fpsyt.2011.00030. [PubMed: 21687771]

Morris LS, McCall JG, Charney DS, and Murrough JW (2020). The role of the locus coeruleus in the generation of pathological anxiety. Brain Neurosci. Adv 4, 2398212820930321. 10.1177/2398212820930321. [PubMed: 32954002]

Napier TC, Chen L, Kashanchi F, and Hu XT (2014). Repeated cocaine treatment enhances HIV-1 Tat-induced cortical excitability via over-activation of L-type calcium channels. J. Neuroimmune Pharmacol 9, 354–368. 10.1007/s11481-014-9524-6. [PubMed: 24567038]

Natarajaseenivasan K, Cotto B, Shanmughapriya S, Lombardi AA, Datta PK, Madesh M, Elrod JW, Khalili K, and Langford D (2018). Astrocytic metabolic switch is a novel etiology for Cocaine and HIV-1 Tat-mediated neurotoxicity. Cell Death Dis. 9, 415. 10.1038/s41419-018-0422-3. [PubMed: 29549313]

Nestler EJ (2014). Epigenetic mechanisms of drug addiction. Neuropharmacology 76 Pt B, 259–268. 10.1016/j.neuropharm.2013.04.004. [PubMed: 23643695]

Norrholm SD, Bibb JA, Nestler EJ, Ouimet CC, Taylor JR, and Greengard P (2003). Cocaine-induced proliferation of dendritic spines in nucleus accumbens is dependent on the activity of cyclin-dependent kinase-5. Neuroscience 116, 19–22. 10.1016/s0306-4522(02)00560-2. [PubMed: 12535933]

Overton PG, Richards CD, Berry MS, and Clark D (1999). Long-term potentiation at excitatory amino acid synapses on midbrain dopamine neurons. Neuroreport 10, 221–226. 10.1097/00001756-199902050-00004. [PubMed: 10203312]

Paris JJ, Carey AN, Shay CF, Gomes SM, He JJ, and McLaughlin JP (2014). Effects of conditional central expression of HIV-1 tat protein to potentiate cocaine-mediated psychostimulation and reward among male mice. Neuropsychopharmacology 39, 380–388. 10.1038/npp.2013.201. [PubMed: 23945478]

Park K, Volkow ND, Pan Y, and Du C (2013). Chronic cocaine dampens dopamine signaling during cocaine intoxication and unbalances D1 over D2 receptor signaling. J. Neurosci 33, 15827–15836. 10.1523/JNEUROSCI.1935-13.2013. [PubMed: 24089490]

Pinheiro JC, and Bates DM (2002). Mixed-Effects Models in S and S-PLUS (Springer).

Pope DA, Boomhower SR, Hutsell BA, Teixeira KM, and Newland MC (2016). Chronic cocaine exposure in adolescence: effects on spatial discrimination reversal, delay discounting, and performance on fixed-ratio schedules in mice. Neurobiol. Learn. Mem 130, 93–104. 10.1016/j.nlm.2016.01.017. [PubMed: 26868477]

Rahimian P, and He JJ (2016). HIV-1 Tat-shortened neurite outgrowth through regulation of microRNA-132 and its target gene expression. J. Neuroinflammation 13, 247. 10.1186/s12974-016-0716-2. [PubMed: 27634380]

Rasakham K, Schmidt HD, Kay K, Huizenga MN, Calcagno N, Pierce RC, Spires-Jones TL, and Sadri-Vakili G (2014). Synapsedensity and dendritic complexity are reduced in the prefrontal cortex following seven days of forced abstinence from cocaine self-administration. PLoS One 9, e102524. 10.1371/journal.pone.0102524. [PubMed: 25072653]

Renthal W, and Nestler EJ (2008). Epigenetic mechanisms in drug addiction. Trends Mol. Med 14, 341–350. 10.1016/j.molmed.2008.06.004. [PubMed: 18635399]

Ribeiro EA, Scarpa JR, Garamszegi SP, Kasarskis A, Mash DC, and Nestler EJ (2017). Gene network dysregulation in dorsolateral prefrontal cortex neurons of humans with cocaine use disorder. Sci. Rep 7, 5412. 10.1038/s41598-017-05720-3. [PubMed: 28710498]

Risher WC, Ustunkaya T, Singh Alvarado J, and Eroglu C (2014). Rapid Golgi analysis method for efficient and unbiased classification of dendritic spines. PLoS One 9, e107591. 10.1371/journal.pone.0107591. [PubMed: 25208214]

Rodriguez-Espinosa N, and Fernandez-Espejo E (2015). Effects of acute and repeated cocaine on markers for neural plasticity within the mesolimbic system in rats. Psychopharmacology (Berl) 232, 57–62. 10.1007/s00213-014-3632-0. [PubMed: 24912888]

Rogge GA, and Wood MA (2013). The role of histone acetylation in cocaine-induced neural plasticity and behavior. Neuropsychopharmacology 38, 94–110. 10.1038/npp.2012.154. [PubMed: 22910457]

Schneider CA, Rasband WS, and Eliceiri KW (2012). NIH Image to ImageJ: 25 years of image analysis. Nat. Methods 9, 671–675. 10.1038/nmeth.2089. [PubMed: 22930834]

Scofield MD, Li H, Siemsen BM, Healey KL, Tran PK, Woronoff N, Boger HA, Kalivas PW, and Reissner KJ (2016). Cocaine self-administration and extinction leads to reduced glial fibrillary acidic protein expression and morphometric features of astrocytes in the nucleus accumbens core. Biol. Psychiatry 80, 207–215. 10.1016/j.biopsych.2015.12.022. [PubMed: 26946381]

Sharma HS, Muresanu D, Sharma A, and Patnaik R (2009). Cocaine-induced breakdown of the blood-brain barrier and neurotoxicity. Int. Rev. Neurobiol 88, 297–334. 10.1016/S0074-7742(09)88011-2. [PubMed: 19897082]

Shen HW, Toda S, Moussawi K, Bouknight A, Zahm DS, and Kalivas PW (2009). Altered dendritic spine plasticity in cocaine-withdrawn rats. J. Neurosci 29, 2876–2884. 10.1523/JNEUROSCI.5638-08.2009. [PubMed: 19261883]

Shu C, Justice AC, Zhang X, Wang Z, Hancock DB, Johnson EO, and Xu K (2020). DNA methylation mediates the effect of cocaine use on HIV severity. Clin. Epigenetics 12, 140. 10.1186/s13148-020-00934-1. [PubMed: 32928285]

Sivalingam K, Cirino TJ, McLaughlin JP, and Samikkannu T (2021). HIV-tat and cocaine impact brain energy metabolism: redox modification and mitochondrial biogenesis influence NRF transcription-mediated neurodegeneration. Mol. Neurobiol 58, 490–504. 10.1007/s12035-020-02131-w. [PubMed: 32978730]

Sun FJ, Wei YJ, Li S, Guo W, Chen X, Liu SY, He JJ, Yin Q, Yang H, and Zhang CQ (2016). Elevated expression of VEGF-C and its receptors, VEGFR-2 and VEGFR-3, in patients with mesial temporal lobe epilepsy. J. Mol. Neurosci 59, 241–250. 10.1007/s12031-016-0714-y. [PubMed: 26798047]

Vainchtein ID, and Molofsky AV (2020). Astrocytes and microglia: in sickness and in health. Trends Neurosci. 43, 144–154. 10.1016/j.tins.2020.01.003. [PubMed: 32044129]

Vorhees CV, and Williams MT (2014). Assessing spatial learning and memory in rodents. ILAR J. 55, 310–332. 10.1093/ilar/ilu013. [PubMed: 25225309]

Wayman WN, Chen L, Napier TC, and Hu XT (2015). Cocaine self-administration enhances excitatory responses of pyramidal neurons in the rat medial prefrontal cortex to human immunodeficiency virus-1 Tat. Eur. J. Neurosci 41, 1195–1206. 10.1111/ejn.12853. [PubMed: 25707266]

Westendorp MO, Frank R, Ochsenbauer C, Stricker K, Dhein J, Walczak H, Debatin KM, and Krammer PH (1995). Sensitization of T cells to CD95-mediated apoptosis by HIV-1 Tat and gp120. Nature 375, 497–500. 10.1038/375497a0. [PubMed: 7539892]

Wiley CA, Baldwin M, and Achim CL (1996). Expression of HIV regulatory and structural mRNA in the central nervous system. AIDS 10, 843–847. [PubMed: 8828741]

Xiao H, Neuveut C, Tiffany HL, Benkirane M, Rich EA, Murphy PM, and Jeang KT (2000). Selective CXCR4 antagonism by Tat: implications for in vivo expansion of coreceptor use by HIV-1. Proc. Natl. Acad. Sci. U S A 97, 11466–11471. 10.1073/pnas.97.21.11466. [PubMed: 11027346]

Yao H, Duan M, Yang L, and Buch S (2012). Platelet-derived growth factor-BB restores human immunodeficiency virus Tat-cocaine-mediated impairment of neurogenesis: role of TRPC1 channels. J. Neurosci 32, 9835–9847. 10.1523/JNEUROSCI.0638-12.2012. [PubMed: 22815499]

Yao H, Kim K, Duan M, Hayashi T, Guo M, Morgello S, Prat A, Wang J, Su TP, and Buch S (2011). Cocaine hijacks σ1 receptor to initiate induction of activated leukocyte cell adhesion molecule: implication for increased monocyte adhesion and migration in the CNS. J. Neurosci 31, 5942–5955. 10.1523/JNEUROSCI.5618-10.2011. [PubMed: 21508219]

Yao WD, Gainetdinov RR, Arbuckle MI, Sotnikova TD, Cyr M, Beaulieu JM, Torres GE, Grant SG, and Caron MG (2004). Identification of PSD-95 as a regulator of dopamine-mediated synaptic and behavioral plasticity. Neuron 41, 625–638. 10.1016/s0896-6273(04)00048-0. [PubMed: 14980210]

Zaqout S, and Kaindl AM (2016). Golgi-cox staining step by step. Front. Neuroanat 10, 38. 10.3389/fnana.2016.00038. [PubMed: 27065817]

Zhai HF, Zhang ZY, Zhao M, Qiu Y, Ghitza UE, and Lu L (2007). Conditioned drug reward enhances subsequent spatial learning and memory in rats. Psychopharmacology (Berl) 195, 193–201. 10.1007/s00213-007-0893-x. [PubMed: 17661018]

Zhang F, Petersen M, Johnson L, Hall J, and O'Bryant SE (2021). Recursive support vector machine biomarker selection for alzheimer's disease. J. Alzheimers Dis 79, 1691–1700. 10.3233/JAD-201254. [PubMed: 33492292]

Zhang Y, Chen K, Sloan SA, Bennett ML, Scholze AR, O'Keeffe S, Phatnani HP, Guarnieri P, Caneda C, Ruderisch N, et al. (2014). An RNA-sequencing transcriptome and splicing database of glia, neurons, and vascular cells of the cerebral cortex. J. Neurosci 34, 11929–11947. 10.1523/JNEUROSCI.1860-14.2014. [PubMed: 25186741]

Zhao X, Fan Y, Vann PH, Wong JM, Sumien N, and He JJ (2020). Long-term HIV-1 tat expression in the brain led to neurobehavioral, pathological, and epigenetic changes reminiscent of accelerated aging. Aging Dis. 11, 93–107. 10.14336/AD.2019.0323. [PubMed: 32010484]

Zhao X, Wilson K, Uteshev V, and He JJ (2021). Activation of alpha7 nicotinic acetylcholine receptor ameliorates HIV-associated neurology and neuropathology. Brain. 10.1093/brain/awab251.

Zhou BY, Liu Y, Kim BO, Xiao Y, and He JJ (2004). Astrocyte activation and dysfunction and neuron death by HIV-1 Tat expression in astrocytes. Mol. Cell. Neurosci 27, 296–305. 10.1016/j.mcn.2004.07.003. [PubMed: 15519244]

Highlights

- Cocaine use worsens impaired learning and memory in brain-specific Tat transgenic mice
- Cocaine/Tat alters gene expression in ECM receptor pathways and microglia
- Cocaine/Tat changes dendritic spines, synaptophysin expression, and glial activation
- Sex and age are both important contributing factors to cocaine and Tat interaction

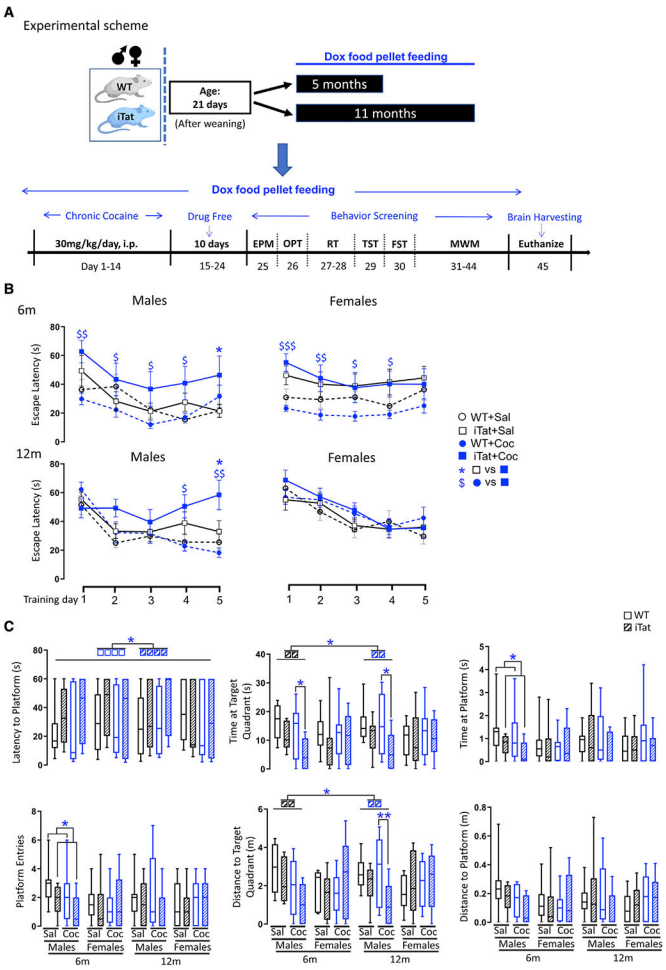

Figure 1. Effects of cocaine on the learning and memory of iTat mice

(A) Experimental scheme. WT and iTat mice were fed with Dox food pellets for 5 or 11 months from day 21 when they were weaned, given cocaine i.p. (30 mg/kg/day) for 14 days, remained drug free for 10 days, and subjected to behavioral assessments: EPM, OPT, RT, TST, FST, and MWM. Dox food pellets continued throughout the studies. Mice were euthanized to collect tissues for pathology or DNA/RNA isolation following MWM.

(B) Escape latency in the MWZ training stages.

(C) Short-term memory from the first probe test demonstrated by Latency to platform, platform entries, time at target quadrant, distance to target quadrant, time at platform, and distance to platform.

n = 8–14/group. $p < 0.05$ was considered significant and marked as * or $ for comparisons among different groups; $p < 0.01$ and $p < 0.001$ were both considered highly significant and marked as ** and ***, respectively. Sal, saline; Coc, cocaine. Error bars: mean ± SEM.

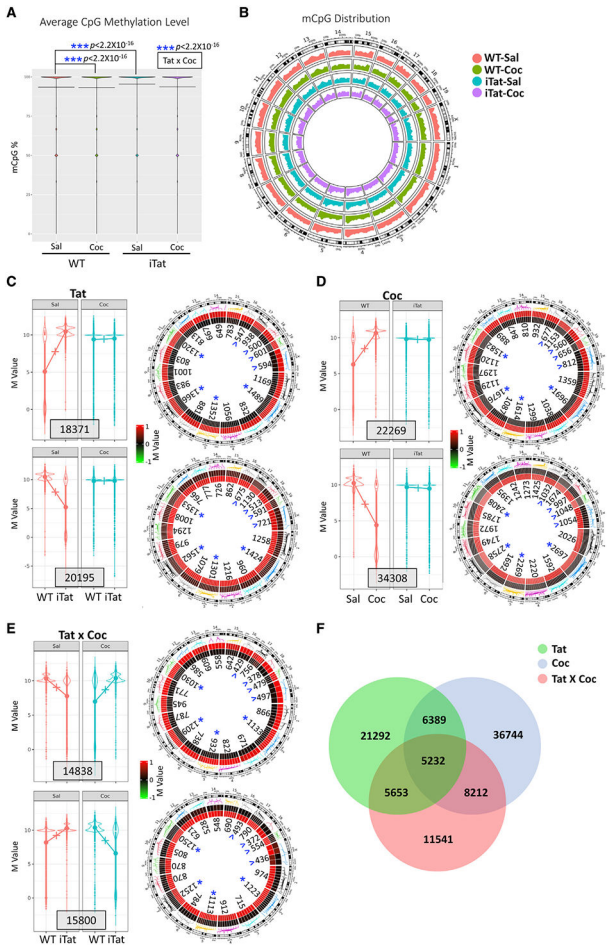

Figure 2. Effects of cocaine on genome-wide DNA methylation in the context of Tat expression

Genomic DNA was isolated from HIP of the mice for genome-wide DNA methylation analysis.

(A) The average CpG methylation level among these four groups (n = 6/group).

(B) The CpG distribution among all mouse chromosomes. Red, WT-Sal; green, WT-Coc; blue, iTat-Sal; pink, iTat-Coc.

(C–F) CpG site-linked differentially methylated regions (DMRs) expressed in M values (left panel) and their chromosomal location (right panel) under factor Tat (WT-Sal versus iTat-Sal) (C), Coc (WT-Sal versus WT-Coc (D), and Tat × Coc (interaction between Tat and Coc) (E). (F) Overlapped DMRs among three comparisons. *Four chromosomes with the top ranked number of up and down DMRs; ∨, four chromosomes with the bottom ranked total number of up and down DMRs.

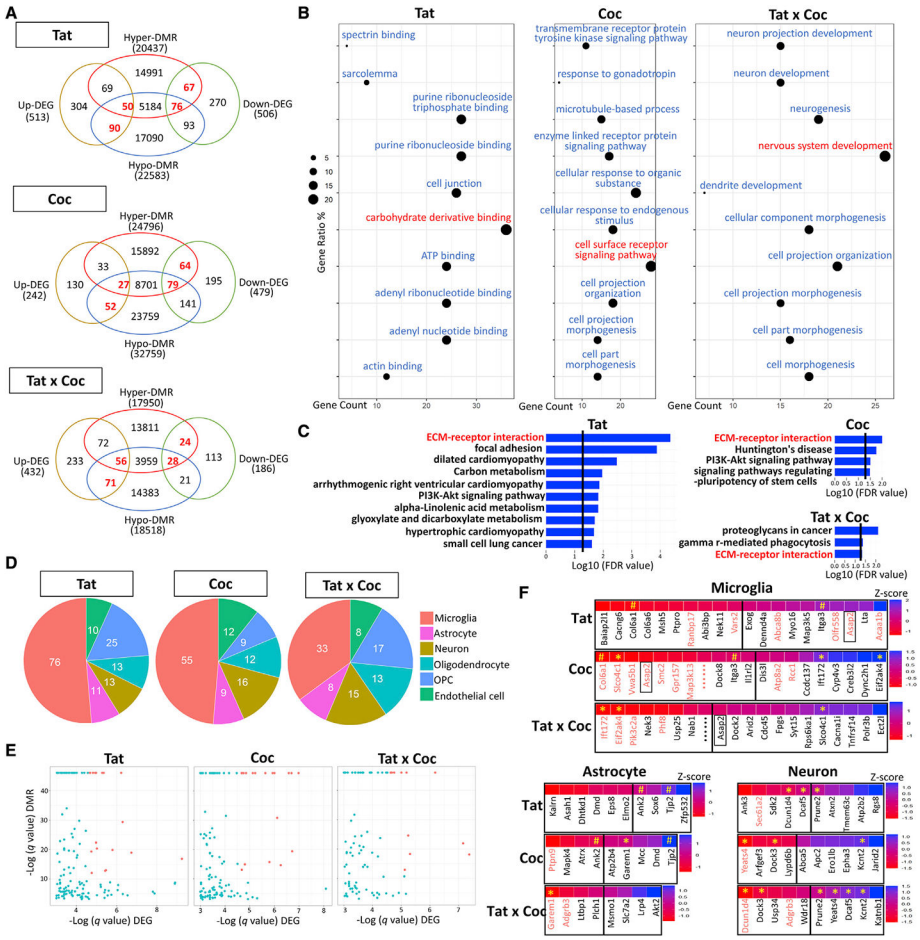

Figure 3. The relationship between CpG DNA methylation and genes expression by each of the factors Tat, Coc, and Tat × Coc

(A–F) RNA was isolated from HIP of the mice and used for RNA-seq analysis. Differentially expressed genes (DEGs) (Up or Down) were identified to be proximal to DMRs (Hyper or Hypo) by each of the factors Tat, Coc, and Tat × Coc (A). Up-DEGs/Hypo-DMR-linked genes and Down-DEGs/Hyper-DMR-linked genes (marked in red) in (Aa) were chosen to run GO (B) and KEGG enrichment analysis (C). The GO cluster with the highest gene ratio and gene count was highlighted in red (B). The extracellular matrix (ECM)-receptor interaction pathway was shared among these three factors (marked in red) in (C). DEGs in each factor were further segregated to different brain cell types: microglia, astrocyte, neuron, oligodendrocyte, oligodendrocyte progenitor cell (OPC), and endothelial cell (D). The most significantly impacted genes that had q < 1e-5 DMRs and q < 0.01 DEGs are marked in red in volcano map (E). Top 20 DEGs with q < 0.05 in microglia and top 10 DEGs with q < 0.05 in astrocytes and neurons were shown in heatmap (F), in which overlapped top genes were marked in white. Red ellipsis, 9330182L06Rik; black ellipsis, 4933407I05Rik. *Genes present in both Tat × Coc and Tat or Coc; #genes present in both Tat and Coc. Framed genes present in Tat, Coc, and Tat × Coc.

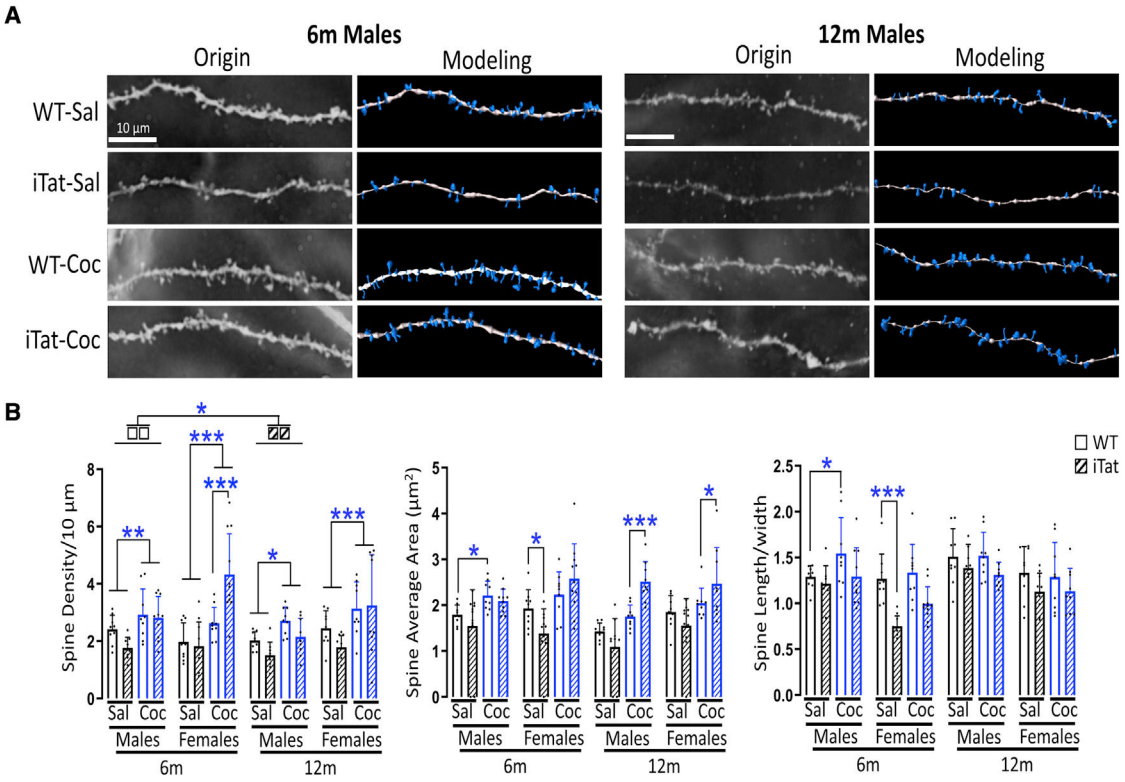

Figure 4. Effects of cocaine on dendritic spine morphology of neurons in HIP of iTat mice

(A and B) Mouse brain sections were stained in the Golgi-Cox solution (A). Scale bar, 10 μm. Dendritic spines in CA1-4 regions were modeled and quantified by Imaris for spine density, occupied area, and length/width.

(B). Representative images (A) were chosen from 6- and 12-month male mice groups. n = 9–11/group. $p < 0.05$ was considered significant and marked as *, and $p < 0.01$ and $p < 0.001$ were both considered highly significant and marked as ** and ***, respectively. Sal, saline; Coc, cocaine. Error bars: mean ± SEM.

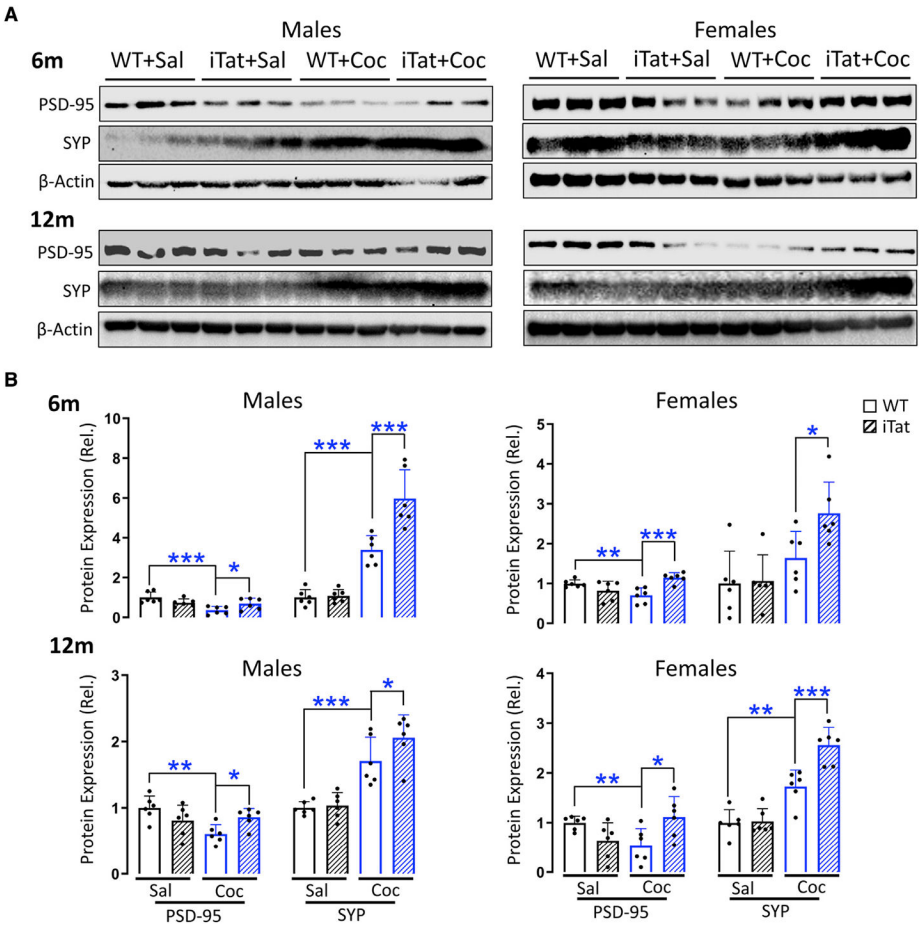

Figure 5. Effects of cocaine on synaptophysin expression in HIP of iTat mice

(A and B) HIP brain regions were dissected from the mouse brain and processed for lysates. SYP and PSD-95 expression in the lysates was determined by western blotting (A), quantified by Fiji, normalized to the loading control β-actin, and calculated using the WT + Sal as a reference, which was set at 1 (B). n = 6/group. $p < 0.05$ was considered significant and marked as *, and $p < 0.01$ and $p < 0.001$ were both considered highly significant and marked as ** and ***, respectively. Sal, saline; Coc, cocaine. Error bars: mean ± SEM.

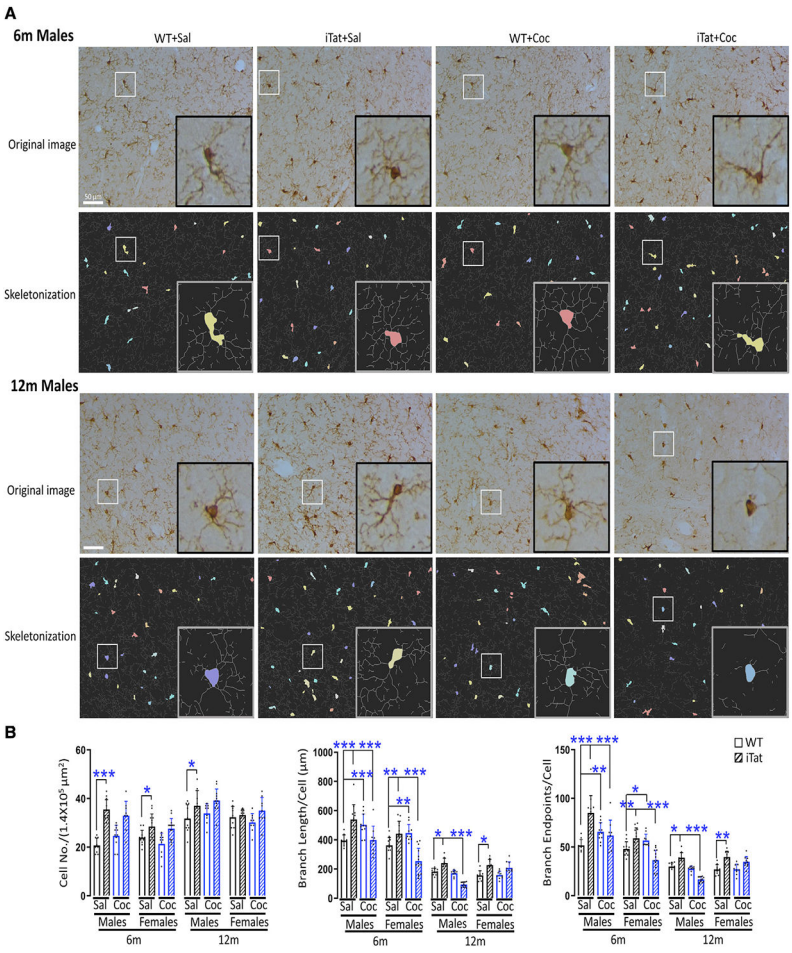

Figure 6. Effects of cocaine on microglia of HIP of iTat mice

Mouse brain sections were stained for Iba-1, the cell bodies of microglia were segmented and the branches were skeletonized by Cellprofiler.

(A) The total number of microglia in every view field (1.4×10^5 μm^2), the branch length of microglia, and the number of the ending points in each microglia were further calculated by Cellprofiler. Scale bars, 50 μm.

(B) Representative images were chosen from 6- and 12-month male mice groups.

n = 9–14/group. $p < 0.05$ was considered significant and marked as *, and $p < 0.01$ and $p < 0.001$ were both considered highly significant and marked as **and ***, respectively. Sal, saline; Coc, cocaine. Error bars: mean ± SEM.

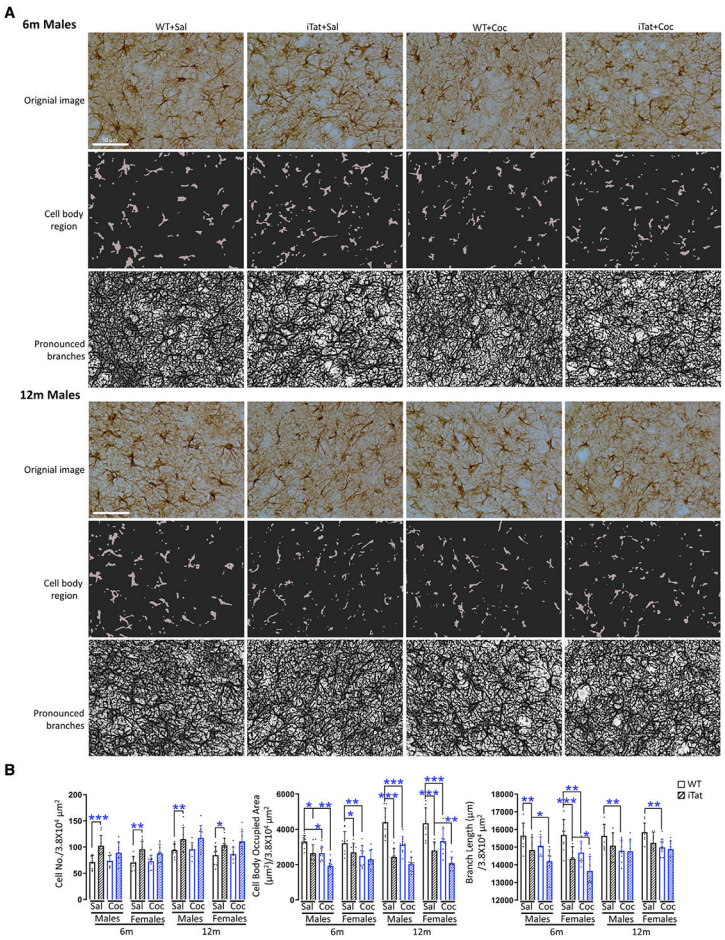

Figure 7. Effects of cocaine on astrocytes of HIP dentate gyrus of iTat mice

Mouse brain sections were stained for GFAP, and the cell bodies of astrocytes in HIP dentate gyrus were segmented and the branches were pronounced by Imaris and ilastik, respectively.

(A) The total number of astrocytes, the cell body occupied area, and the branch length were further calculated by Imaris or Cellprofiler in every view field (3.8×10^4 μm^2). Scale bars, 50 μm.

(B) Representative images were chosen from 6- and 12-month male mice groups.

n = 9/group. $p < 0.05$ was considered significant and marked as *, and $p < 0.01$ and $p < 0.001$ were both considered highly significant and marked as ** and ***, respectively. Sal, saline; Coc, cocaine. Error bars: mean ± SEM

KEY RESOURCES TABLE

REAGENT or RESOURCE	SOURCE	IDENTIFIER
Antibodies		
Iba-1 (1:800)	Wako	Catalog # 019–19741; RRID: AB_839504
GFAP (1:500)	DAKO	Catalog # Z0334; RRID: AB_10013382
NeuN (1:500)	Millipore-sigma	Catalog # MAB377; RRID: AB_2298772
PSD-95 (1:2000)	Abcam	Catalog # Ab18258; RRID: AB_444362
Synaptophysin (1:1000)	Abcam	Catalog # Ab8049; RRID: AB_2198854
β-actin (1:2000)	Sigma-Aldrich	Catalog # A1978; RRID: AB_476692
Goat anti-rabbit secondary antibody, HRP (1:200)	Southern Biotech	Catalog # 4030–05; RRID: AB_2687483
Goat anti-mouse secondary antibody, Alexa 488 (1:500)	ThermoFisher	Catalog # A11001; RRID: AB_2534069
Chemicals, peptides, and recombinant proteins		
Dox food pellets (0.625g/kg)	Envigo	Catalog #TD.01306
Protease inhibitors	Millipore-Sigma	Catalog # S8830
TRIzol reagent	ThermoFisher	Catalog # 15596026
Critical commercial assays		
DAB kit	Abcam	Catalog # Ab103723
DNeasy Blood & Tissue Kit	Qiagen	Catalog # 69504
Bio-Rad DC protein assay kit	Bio-Rad	Catalog # 5000111
Pico Methyl-Seq Library Prep Kit	ZYMO	Catalog # D5456
RNA Clean & Concentrator Kit	ZYMO	Catalog # R1013
QIAseq Stranded mRNA Select kit	Qiagen	Catalog # 180773
Deposited data		
WGBS and RNA-seq data	This paper	GSE200255: https://www.ncbi.nlm.nih.gov/geo/query/acc.cgi?acc=GSE200255
Experimental models: Organisms/strains		
Wild-type (C57BL/6) mouse	Jackson Laboratory	Strain # 000664
iTat mouse	This Study	N/A
Software and algorithms		
nf-core/methylseq	Ewels et al. (2020)	https://nf-co.re/methylseq
FASTQC (v 0.11.9)	N/A	http://www.bioinformatics.babraham.ac.uk/projects/fastqc/
Trim Galore! (v0.6.5)	N/A	http://www.bioinformatics.babraham.ac.uk/projects/trim_galore/
Bismark (v0.22.3)	Krueger and Andrews (2011)	https://www.bioinformatics.babraham.ac.uk/projects/bismark/
Bowtie2 (v2.4.2)	Langmead and Salzberg (2012)	http://bowtie-bio.sourceforge.net/bowtie2/index.shtml
R program (version 4.0.4)	N/A	http://www.r-project.org
annotatr package	Cavalcante and Sartor (2017)	https://bioconductor.org/packages/release/bioc/html/annotatr.html
STAR (v2.7.9)	Dobin et al. (2013)	https://github.com/alexdobin/STAR
featureCounts (v2.0.1.13)	Liao et al., 2014	http://subread.sourceforge.net/
annotatr package	Cavalcante and Sartor (2017)	https://pubmed.ncbi.nlm.nih.gov/28369316/
DAVID (v6.8)	Huang et al. (2009)	https://david.ncifcrf.gov/

REAGENT or RESOURCE	SOURCE	IDENTIFIER
Support Vector Machine	Zhang et al. (2021)	https://pubmed.ncbi.nlm.nih.gov/33492292/
Anymaze (V6.1)	Stoelting	N/A
Image J	Schneider et al. (2012)	https://imagej.net/downloads
Imaris	Bitplane	N/A
Ilastik	Berg et al. (2019)	https://www.ilastik.org/
Cellprofiler	McQuin et al. (2018)	https://cellprofiler.org/
SPSS (v20)	IBM	https://www.ibm.com/analytics/spss-statistics-software
Other		
polyvinylidene fluoride membrane (0.45 μm)	GE Healthcare Life Sciences	catalog # 10600023
MQ beads	Epigentik	catalog # P-1059
EPM apparatus	San Diego Instruments	Part # 7001–0336
OPT acrylic chamber	San Diego Instruments	Part # 7001–0354
IITC Rotarod	San Diego Instruments	Part # 2360–0143
Morris water maze	San Diego Instruments	Part # 7000–0723
Nanodrop	ThermoFisher	catalog #13-400-518
Qubit 4 Fluorometer	ThermoFisher	catalog # Q33238